Recent Developments in Copper-Based Catalysts for Enhanced Electrochemical CO_2 Reduction

Recent Developments in Copper-Based Catalysts for Enhanced Electrochemical CO_2 Reduction

Manova Santhosh Yesupatham[a†], Brahmari Honnappa[b†], Nithish Agamendran[a], S. Sai Yeswanth kumar[a], Gayathri Chellasamy[c], Saravanan Govindaraju[c], Kyusik Yun[c] , N. Clament Sagaya Selvam[a*], Arthanareeswari. M[a*], Wei Li[d*], Karthikeyan Sekar[a,d*]

[a]Sustainable Energy and Environmental Research Laboratory, Department of Chemistry, Faculty of Engineering and Technology, SRM Institute of Science and Technology, Kattankulathur 603203, India.

[b]Department of Physics and Nanotechnology, SRM Institute of Science and Technology, Kattankulathur 603203, Tamil Nadu, India.

[c]Department of Bionanotechnology, Gachon University, Gyeonggi-do 13120, Republic of Korea.

[d]School of Engineering, Institute for Materials & Processes, The University of Edinburgh, Robert Stevenson Road, Edinburgh EH9 3FB, United Kingdom.

Corresponding author: E-mail: Karthiks13@srmist.edu.in

Abstract

The drastic climate change imposing adverse environmental effects has received serious research attention for finding a suitable solution. The replacement of conventional fossil energy sources with renewable and sustainable energy sources is the potential route and thus manifests as a viable solution. Accordingly, the electrocatalytic CO_2 reduction process coupled with the renewable energy source is an emerging strategy for adopting a sustainable approach. However, the existing challenges in designing suitable catalyst, support material, electrolyte, inadequate selectivity, and intermediate reactions of CO_2 reduction demands substantial research advancement. Numerous studies have been reported for the CO_2 reduction process highlighting the importance of catalyst design and product selectivity. Importantly, the copper-based catalysts, capable in the output of multi-carbon products, have been reported as a "star" material. This review, therefore, focuses on catalyst design strategies, unique structural/morphological features, and product selectivity of diverse copper-based catalysts. The outstanding findings of copper-based catalysts and the corresponding products are critically discussed with adequate figures of merits. The impact of structural/morphological features on product selectivity is discussed in detail. The future scope and our perspectives on copper-based catalysts for the feasible electrocatalytic CO_2 reduction application is summarised.

Keywords: Copper-Based Catalysts, Electrochemical, CO_2 Reduction, multi-carbon (C2+) products, Product selectivity

1. Introduction

Electrocatalytic conversion of carbon dioxide for the Paris goals

The energy crisis is due to the depletion of non-renewable resources, when they are utilized, they not only cause global warming but also produce large amounts of carbon dioxide and lead to greenhouse gas effects.[1] Efforts have been taken to reduce the production of greenhouse gas (CO_2).[2] An international deal on climate change known as the Paris Agreement was approved by 196 countries by the middle of December 2015, and it took effect by the start of November 2016, with a ultimate goal is to limit global warming which is to decrease the temperature below 1.5 °C.[3] In 2016, it was noted that the concentration of CO_2 has increased to a large extent of 400 ppm of the whole atmosphere and demands have been raised to convert CO_2 to other forms of carbonaceous chemicals or fuels, this leads to the sustainability and development of human society.[4] Though industries have been consuming large amounts of fossil fuels and producing CO_2, which causes anthropogenic effects, these emissions cause global warming and health hazards on the biological species which impacts sustainability.[5] The levels of CO_2 have increased from 280 ppm to 400 ppm in the last ten years and there is a possibility, it may rise to 700 ppm at the end of this century.[6] On the other hand, CO_2 production into the atmosphere has been a threat, but it is essential for the production of electricity, daily needs, and industrial applications. So, the excess CO_2 must be converted into valuable fuels, carbonaceous and sustainable products as displayed in **(Fig.1)**.[6c, 7]

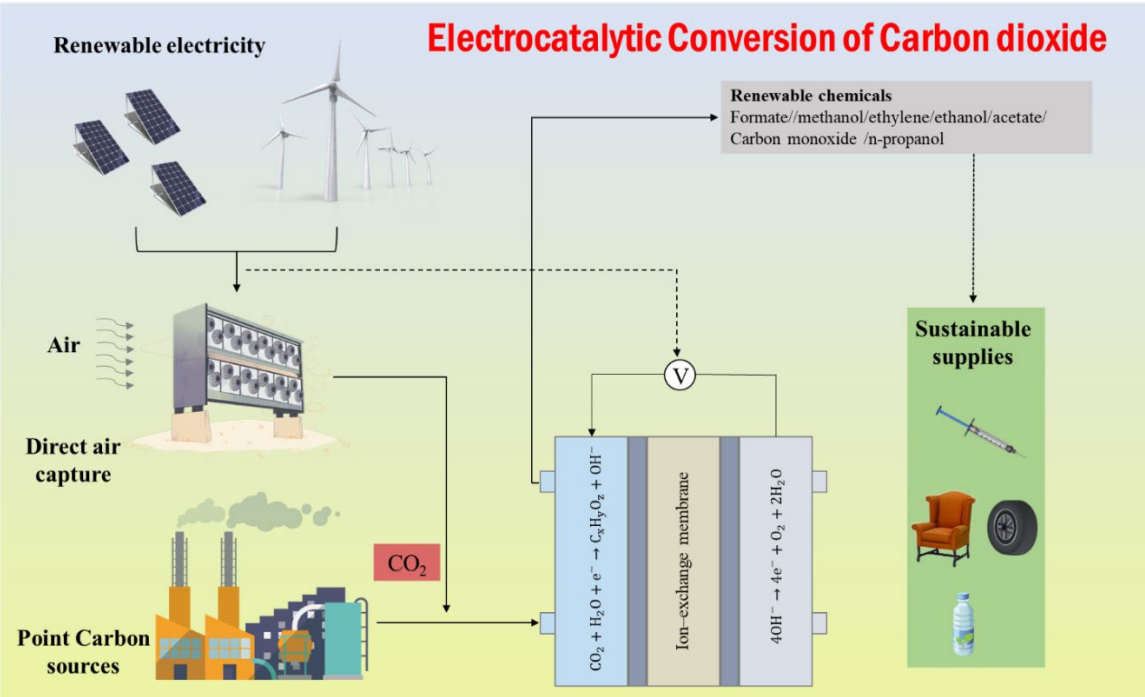

Fig.1 A straightforward approach towards environmentally friendly and sustainable supplies for electrocatalytic conversion of CO_2.

The conversion of CO_2 into other useful fuels is an innovative method to reduce the carbon dioxide in the ecosystem and thus decreasing the level of CO_2 in the atmosphere.[8] CO_2 has two carbonyl groups with double bonds having shorter bond length (116 ppm).[9] CO_2, is a molecule thermodynamically stable. There are substantial technological challenges in the conversion process, specifically in catalytic reduction. Note that the reduction can be of the photochemical, electrochemical, thermochemical and biochemical methods.[10] The electrocatalytic method has been a promising approach due to its good efficiency and high reaction rate in ambient conditions. Moreover, the electrocatalytic approach driven by carbon-free sources (solar energy and wind energy), but it requires high cost and still produce low-efficiency products, due to this major drawback.[11] Electrocatalytic reduction (ECR) has been a prior choice as we can form selective products by using the preferable catalysts.[12] But the challenge in the carbon dioxide reduction is to overcome the kinetic energy (KE) barrier as the onset potential/overpotential is more negative than standard reduction potential (SRP).[13] Although when aqueous electrolytes are reduced and hydrogen is evolved, this is also called Hydrogen Evolution Reaction (HER), thus the electrocatalysts used should accelerate ECR to produce specific products and suppress HER.[14] Different electrocatalysts have been used for the various ECR applications.[15] Among them are homogenous catalysts, which include transition metal complexes that mimic the natural photosynthetic system and yield specific products.[16] However, heterogeneous electrocatalysts are simple to separate and have a low production cost, which has attracted remarkable research attention for CO_2 reduction.[17] Although the heterogeneous electrocatalyst now uses multi-electron transfer methods to produce products like formate and metals like Zn, Au, and Ag have a high affinity for *COOH to produce carbon monoxide.[18] Metals like Sn, Bi, and Pb that have a low affinity for CO_2 to generate formic acid or formate.[19] Thus, the choice of an earth-abundant and non-precious metal will be an ideal choice for CO_2 reduction.[20]

In this regard, Cu-based materials represent the only class of electrocatalysts in which the reduction of CO_2 gives hydrocarbons and alcohols with good efficiency and selectivity.[21] Copper is an abundant metal and its derivatives have strong potential in the reduction of CO_2 into different valuable products.[22] Therefore, synthesis, developing of copper nanostructures, and CO_2 reduction reaction pathways needs to be highlighted. Further, addressing the conditions for potentially executing the CO_2 reductions and the challenges associated must be focussed.

The products for different electron transfers are listed below **(Table 1)**.

Table 1. Standard Potential for CO_2 Electroreduction Reactions in Aqueous Media at 25°C.

Product name	E^0(V vs. RHE)	Reaction
Carbon monoxide	-0.10	$CO_2 + 2H^+ + 2e^- \rightarrow CO_{(g)} + H_2O$
Formic acid	-0.12	$CO_2 + 2H^+ + 2e^- \rightarrow HCOOH_{(aq)}$
Methanol	0.03	$CO_2 + 6H^+ + 6e^- \rightarrow CH_3OH_{(aq)} + H_2O$
Methane	0.17	$CO_2 + 8H^+ + 8e^- \rightarrow CO_{4\,(g)} + 2H_2O$
Graphite	0.21	$CO_2 + 4H^+ + 4e^- \rightarrow C_{(s)} + 2H_2O$
Oxalic acid	-0.47	$2CO_2 + 2H^+ + 2e^- \rightarrow (COOH)_{2\,(s)}$
Acetic acid	0.11	$2CO_2 + 8H^+ + 8e^- \rightarrow CH_3COOH_{(aq)} + 2H_2O$
Acetaldehyde	0.06	$2CO_2 + 10H^+ + 10e^- \rightarrow CH_3CHO_{(aq)} + 3H_2O$
Ethanol	0.09	$2CO_2 + 12H^+ + 12e^- \rightarrow C_2H_5OH_{(aq)} + 3H_2O$
Ethylene	0.08	$2CO_2 + 12H^+ + 12e^- \rightarrow C_2H_{4_{(g)}} + 4H_2O$
Ethane	0.14	$2CO_2 + 14H^+ + 14e^- \rightarrow C_2H_{6_{(g)}} + 4H_2O$
Propionaldehyde	0.09	$3CO_2 + 16H^+ + 16e^- \rightarrow C_2H_5CHO_{(aq)} + 5H_2O$
Propanol	0.10	$3CO_2 + 18H^+ + 18e^- \rightarrow C_3H_2OH_{(aq)} + 5H_2O$

The above **table.1** shows that the products formed are two carbon products (C_2) more than one carbon products (C_1) products, the C_2 products have higher potentials with considerable energies.

Experts have developed catalysts that bypasses the carbon anion radical and uses multi-proton multi-electron transfer to reduce CO_2 at low energy costs.[23] ECR is carried out with a suitable electrocatalyst at a particular reduction potential.[24] In most cases, the carbon anion radical $CO_2^{\cdot-}$ is formed and it is unfavourable due to the negative redox potential of -1.90 V in water. As demonstrated in **table 1**, CO_2 can be reduced into a variety of useful products at different potentials.[25] These products are generated under neutral conditions as opposed to the provided conventional Normal Hydrogen Electrodes (NHE). The **table 1** displays a variety of products, and equation for hydrogen evolution by a two-electron mechanism that competes with CO_2 reduction. These reactions have high over potentials and thus ECR is a highly competitive process to hydrogen evolution in water splitting, therefore products with specific selectivity can be produced.[26] However, the ECR has been challenging due to the larger overpotential of the carbon

dioxide, which leading to decrease the product efficiency and selectivity.[27] It has been demonstrated that it is effective to control the various morphology of nanostructured metal catalysts.[28] However, the foremost problem is the weak adsorption of CO_2 on the surface of catalysts and poor solubility. To enhance the solubility and adsorption on metal catalysts, co-catalysts or sorbents such as aqueous electrolytes, nitrogen-containing polymers and organic molecules are used. But the main problem is expensive catalysts, the procedures are complicated, and the liquid products are not easily separable.[29] Copper that has been modified with other elements, planar and nanostructured copper, as well as theoretical and experimental techniques are all included in ECR.[30] It intends to include all investigations on ECR in liquid electrolytes employing copper employing catalysts, commencing from numerous earlier researches from 1980s until the 1990s and finishing with those published in 2018.[31]

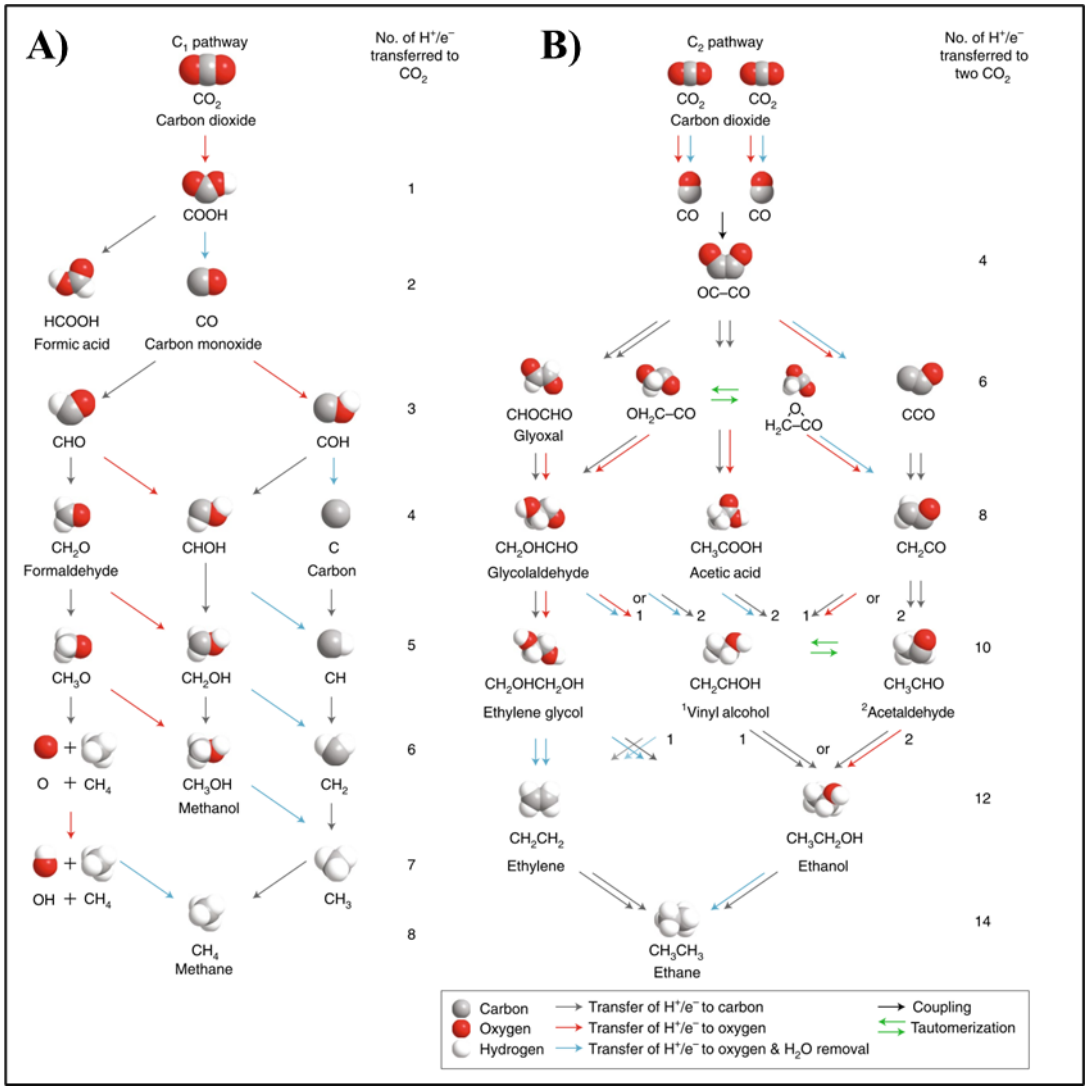

Fig.2 Illustration of a molecular model showing potential CO_2RR formation pathways for different C_1 and C_2 products. According to the quantity of H^+ and e^- pairs exchanged, these pathways lead to C_1 products (through CO intermediate; A) and C_2 products (by CO dimerization; B). H^+ and e^- transfer to either carbon

or oxygen sites are shown by coloured arrows, according to the legend. Known products bear their common name and chemical information. (Reproduced from ref [26] with consent from the Nature Catalysis, copyright 2021).

In this review, we highlight the potential of copper-based catalyst for the reduction of CO_2. We also discuss the importance and need for the reduction of CO_2. The selective nature of copper on selectivity of CO_2 based products was then discussed, along with the difficulties and futuristic facets of this incredibly intriguing material. We anticipate this systematically presented review will enlighten the readers with recent progress and role of copper-based catalysts for the reduction of CO_2.

2. Why CO_2 Recycling Is Important

The "industrial metabolism" of human civilisation, including our energy infrastructures and chemical industries, is fundamentally based on the oxidation of carbon.[30] Carbon reduction is still lacking in human industrial metabolism, whereas CO_2 reduction in photosynthesis balances CO_2 in aerobic respiration in biological metabolism.[32] Reducing CO_2 emissions is critical in our efforts to combat climate change, and plants play a vital role in this endeavour. For thousands of years, plants have employed photosynthesis to convert carbon dioxide (CO_2) into energy-rich chemicals (carbohydrates), helping nature to keep its very own carbon cycle and provide mankind with a stable ecosystem. The current situation of global warming and climate change cannot be tackled with natural CO_2 reduction method, and so an innovative solution is needed. Electrocatalysis is one such solution which offers a more controlled and scalable approach to CO_2 reduction. By using renewable energy sources and advanced catalysts, electrocatalytic processes can efficiently convert CO_2 into valuable chemical compounds, reducing our carbon footprint and offering a versatile pathway to reduce atmospheric CO_2 levels. Combining the natural benefits of trees with cutting-edge electrocatalytic technologies holds promise for a more sustainable and impactful approach to CO_2 reduction shows in **(Fig.3)**.

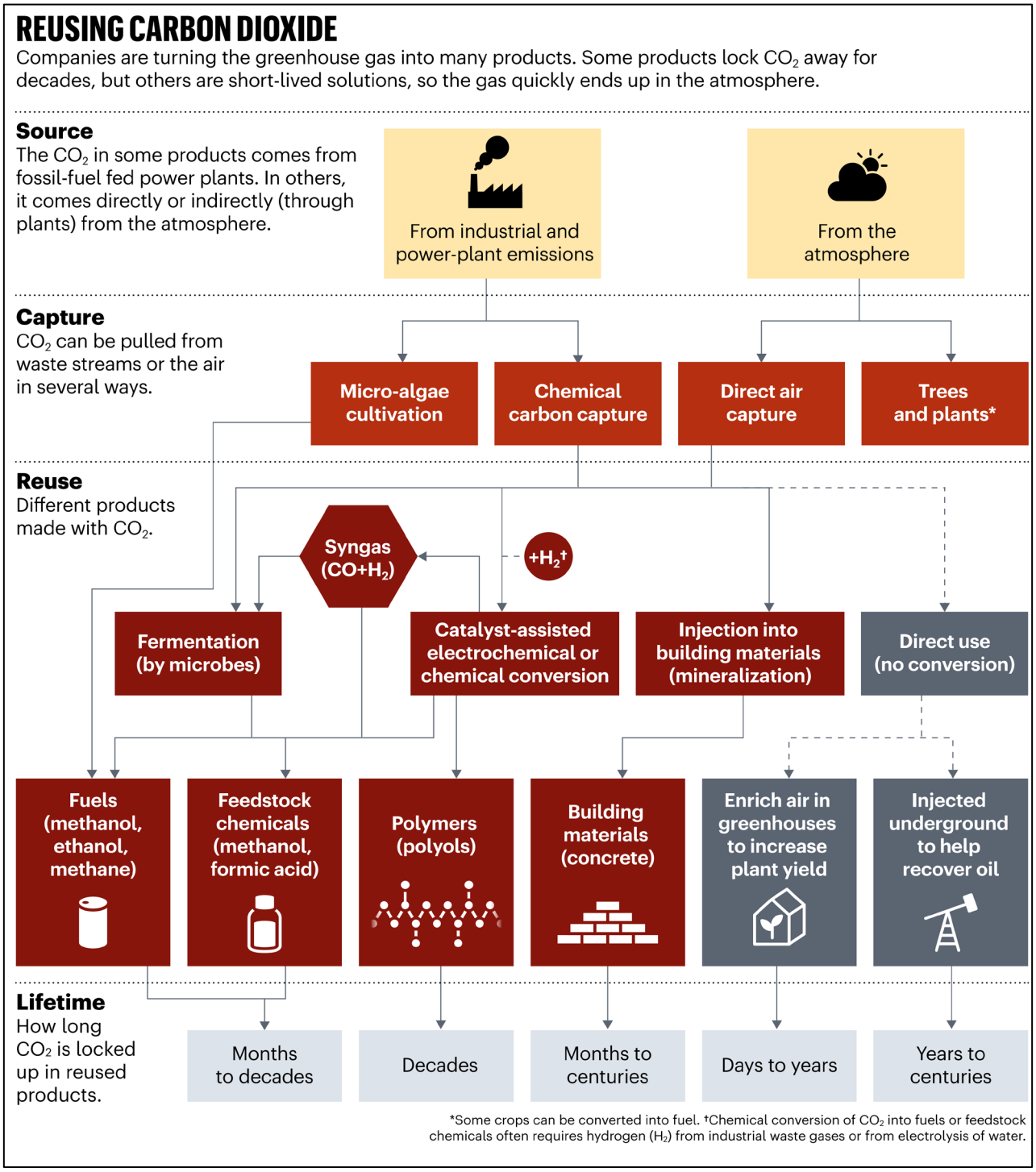

Fig.3 Schematic representation displaying several products are being created by businesses using the greenhouse gas. While some products keep CO_2 trapped away for decades, others are only temporary solutions, allowing the gas to soon enter the environment (Reproduced from ref [33] with consent from the Nature , copyright 2021).

First, we will briefly discuss decarbonization, carbon sequestration, and the other important CO_2 recycling possibilities to give some context for the larger picture. Since the 1860s, when the industrial revolution

began, and especially in the last two decades, when urbanisation has increased at an exponential rate, carbonaceous emissions have increased dramatically, leading to much of the extraordinary global warming of the previous decade.[34] But massive human-caused or industrial emissions of carbon dioxide (CO_2), an invisible greenhouse gas, cause a far more severe and toxic atmosphere. An undesirable side effect of industrialization and development over the past few decades has been the use of excess fossil fuels that has accumulated over many millions of years.[35] The Conference of Parties, or COP21, of the United Nations Framework Convention on Climate Change (UNFCC) gathered for the 21st session this year in Paris.[36] In order to maintain the post-industrial world temperature, rise below 2 °C, policy analysts, researchers, and environmental economists from 118 nations voluntarily committed to adopt steps to combat global warming at COP21.[37] Carbon emissions taxes or increased gas taxes are another option for encouraging people and businesses to reduce their energy consumption and their impact on the environment. The Clean Power Plan is a set of regulations put in place by the Environmental Protection Agency which targets the percentage of carbon emissions which is let out from the power plants. The strategy to reduce carbon dioxide emissions from power plants in 2015 was developed by United States (US).[38] To meet these goals, choosing an ideal catalyst is crucial. Now we discuss about the criteria to employ copper as a catalyst for reduction of CO_2.

3. Choice of Catalyst

Researchers have known since the 1970s that copper has a unique capacity to convert carbon dioxide into useful compounds and fuels. However, for many years, researchers have battled to comprehend how this ubiquitous metal functions as an electrocatalyst, a device that harnesses electron energy to change molecules into other chemicals.[39] Many electrocatalyst exists, but copper existing as an electrocatalyst produce various hydrocarbons and alcohols through electrochemical CO_2 reduction, the various factors influencing copper to be a good electrocatalyst inducing efficient electrochemical reduction of CO_2 includes morphology, composition, selectivity, choice of electrolyte, etc. The first CO_2RR was reported in the year 1950.[40] Hori and co-workers reported hydrocarbon-based qualification of CO_2RR with faradic efficiency of 100 percent.[41] The CO_2RR was performed on various polycrystalline electrodes at a current density of 5 mA/cm^2 in a 0.5 M $KHCO_3$ solution, similarly the following studies have been carried out with four groups of metal electrodes on the basis of the reaction products obtained, the first group includes catalysts such as Bi, Tl, Pb, Hg, In, Sc and Cd, the next group includes catalyst such as Au, Ag, Ga, Pd, and Zn, the third set includes Fe. Ni, Pt and Ti. The first group produces formate as prime product, the second group produce CO as major product, and the third group readily binds with hydrogen and excludes the reduction of CO_2. Furthermore, the element Cu exists as a separate element from other elements due to its novelty in formation of the hydrocarbon and alcohol products. Cu existing as a non-precious metal and it can produce valuable chemicals efficiently via two-electron mechanism and a major perk of using Cu as catalyst, is it

can achieve minimum current density of 5 mA/cm^2 which other catalysts cannot achieve without giving needed overpotential. Cu catalysts produce efficient electrocatalytic performance in CO_2RR with a moderate potential of -1.04 V vs RHE (Reversible Hydrogen Electrode). Copper versatility as an electrochemical catalyst for CO_2 reduction allows it to convert CO_2 into a variety of useful chemicals, including carbon monoxide, formic acid, methane, and ethylene.[42] Cu's versatility for diverse applications is demonstrated by the fact that the selectivity towards particular products can be modified by modifying variables like electrode voltage, pH, and surface shape. The key factors driving CO_2 reduction reactions are the creation of copper hydride intermediates and the presence of certain surface locations. Cu many reaction routes provide opportunities for improving catalyst performance and product selectivity. These pathways are made possible by Cu redox characteristics. The path to Cu-based catalysts for CO_2 reduction is not without obstacles, though the selectivity and effectiveness of CO_2 reduction are frequently hampered by competing HER.[43] In order to maximise selectivity towards target goods while minimising HER interference, researchers are continuously looking for solutions. The study also emphasises how crucial catalyst stability is to real-world applications. Cu catalysts are prone to changes in oxidation state and structural alterations during catalysis, which eventually results in deactivation. In order to solve stability issues and extend catalytic lifetimes, techniques including nano structuring, alloying, and composite catalysts are being investigated. Achieving high-performance Cu catalysts clearly highlights the significance of catalyst design and engineering. Underscoring the significance of surface science and materials engineering in this area, researchers may modify the catalytic behaviour and selectivity by manipulating crystal facets, surface flaws, and nanoparticle shape. The amazing capacity of copper to control the reduction route, resulting in the output of specific products, is at the core of copper catalysis. The CO_2 reduction reaction can be directed towards desired products by carefully adjusting reaction parameters, such electrode, voltage and pH. This selectivity control is essential for adjusting the performance of the catalyst to match the needs of certain applications, from the synthesis of chemical feedstocks to the storage of renewable energy. Copper catalyst surface engineering is found to be a crucial determinant of catalytic results. Copper nanoparticles with its shape, crystal facets, and defect density have a significant impact on the kinetics and selectivity of reactions. These catalysts exposed surfaces and active sites direct CO_2 molecules adsorption and activation, eventually directing the reaction into certain product routes. The thermodynamic potential and selectivity of CO_2RR for metal catalysts are often influenced by the metals ability to bind to the adsorbed CO_2 or CO. Due to the peculiar electronic structure of Cu, which is the sole metal to do so in comparison to other metals, C_2H_4 is produced more easily. The surface releases the metal with a low CO binding energy before further CO reduction took place as the metal first converted to CO from CO_2 at the surface, whereas metals with a high CO binding strength would combine with CO. Because the metal sites coupled to CO prevent them from moving on to the next stage of CO_2 catalysis, the

hydrogen evolution ($2H_2O + 2\,e \rightarrow H_2 + 2\,OH$) dominates. Due to its thermodynamic potentials for all half-cell CO_2RRs, HER in an aqueous electrolyte is invariably a competitive side reaction with CO_2RR was shown in **(Fig.4)**. The greatest documented FE of C_2H_4 in an H-type cell is currently reported to be 80%, which is much less than the approximately 100% efficiency of C_1 products (CO, HCOOH, etc.). Additionally, the current density of C_2H_4 is often less than 10 mA/ cm^2, which is below the 200 mA/ cm^2 threshold for industrial applications.[44]

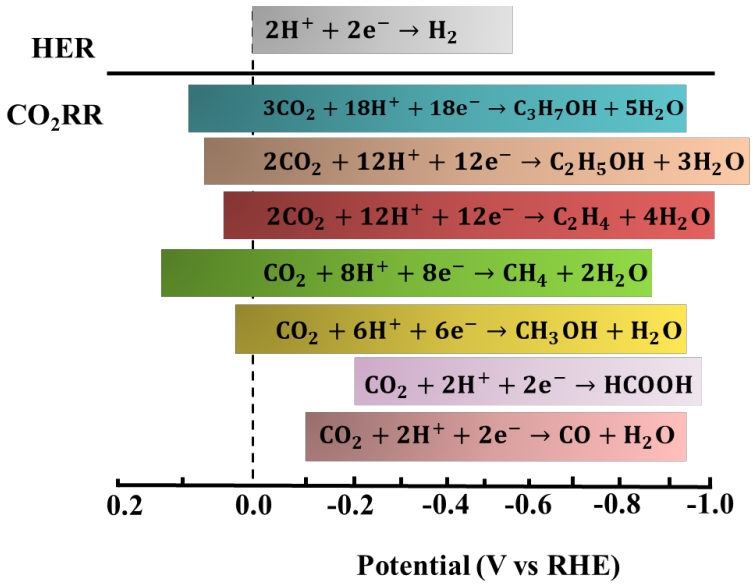

Fig.4 Thermodynamic potentials of hydrogen evolution reaction and CO_2RR in aqueous electrolyte with standard situations.

Cu-based materials, such as nano copper, copper alloy, copper oxide, copper sulphide, copper nitride, and others, exhibit a distinctive electrocatalytic favouritism for C_2H_4, which has been examined as a model catalyst.[45] The exceptional electrocatalytic activity of Cu-based materials can be attributed to the *CO intermediate favourable binding energy, which promotes the C-C coupling process. It is widely acknowledged that C-C association is an important process in the production of C_2H_4. Cu-based catalyst performance is often influenced by a variety of factors, including shape, surface state, crystal defects, phases, and so on. These variables contribute to change the potential for important chemical intermediates to occur, the reactant's concentration close to the electrode, the pH of the electrolyte, and other variables.

Simultaneously, high performance catalysts—that is, with high faradic efficiency and current density for a particular product—are needed for ECR commercial uses. These catalysts must also be stable over the long run. However, compared to activity/selectivity difficulties, the catalyst structural stability in ECR circumstances has received significantly less attention. Even while steady operating lengths of up to 150 hours have been observed, performance degradation is already evident in a few tens of minutes for some

Cu-based catalysts. Research on catalyst failure mechanisms has been sparse in comparison to studies on other important electrochemical events, such as reduction and evolution reactions. We observe that there is, in general, a lack of a methodical and critical review of the stability of Cu-based catalysts for ECR.

The road to using copper catalysis for CO_2 reduction is not without its difficulties, though CO_2 reduction technologies frequently lose efficiency and selectivity due to competing HER. Innovative approaches are needed to address this problem, such as developing better electrolyte formulations or creating catalyst structures that inhibit HER. Copper is a flexible and fascinating candidate in the field of CO_2 reduction catalysis. Its promise for transforming CO_2 into useful chemicals is highlighted by its ability to direct complex electrochemical processes and tailor surface characteristics. To fully realise the potential of copper-based catalysts for a more sustainable future, researchers are expected to develop novel solutions to problems including selectivity enhancement and stability improvement.

4.Copper-based catalyst for C_1 and C_{2+} products:

When Cu is used as the electrocatalyst, CO_2 is converted to the products C_1 and C_{2+}. The molecules with just one carbon in their molecular formula, such as CO, HCOOH, CHO, CH_4, and others, are known as C_1 products. Compounds with more than one carbon in their molecular formula, such as C_2H_5OH, C_2H_4, and so forth, are known as C_2 and C_{2+} products. The **(Fig.5)** depicts the formation of C_1, C_2 and C_{2+} products using Cu as the catalyst.

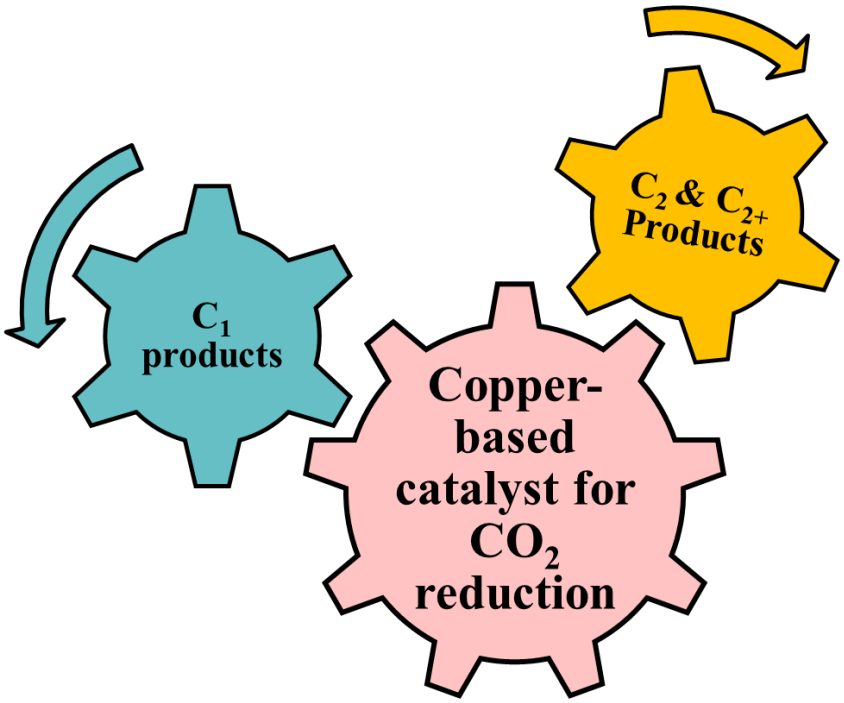

Fig.5 Pictorial representation of copper-based catalyst for electrocatalytic CO_2RR into C_1 and C_{2+} products.

Furthermore, we discuss about the progress of copper-based catalyst that has been used to reduce CO_2 to C_1 products.

4.Copper-based catalyst for C_1 and C_{2+} products:

When Cu is used as the electrocatalyst, CO_2 is converted to the products C_1 and C_{2+}. The molecules with just one carbon in their molecular formula, such as CO, HCOOH, CHO, CH_4, and others, are known as C_1 products. Compounds with more than one carbon in their molecular formula, such as C_2H_5OH, C_2H_4, and so forth, are known as C_2 and C_{2+} products. The **(Fig.5)** depicts the formation of C_1, C_2 and C_{2+} products using Cu as the catalyst.

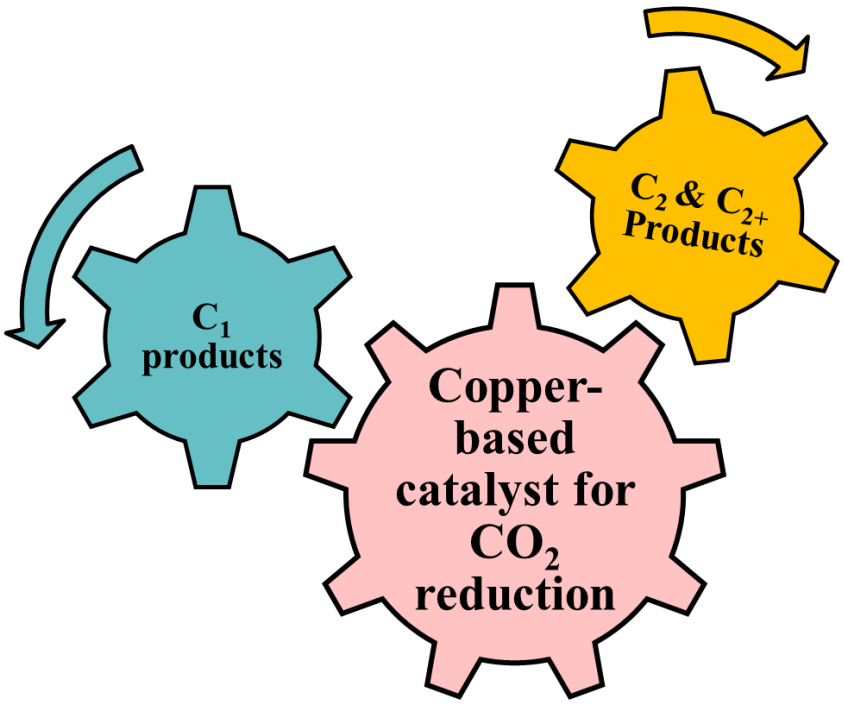

Fig.5 Pictorial representation of copper-based catalyst for electrocatalytic CO_2RR into C_1 and C_{2+} products.

Furthermore, we discuss about the progress of copper-based catalyst that has been used to reduce CO_2 to C_1 products.

4.1 Copper-based catalyst for C_1 product:

Mengchu Wang and co-workers[46] have reported a copper-based electrocatalyst for electrochemical reduction of CO_2 to C_1 products, here in multiwalled carbon nanotubes (MWCNTs) are used to modulate the selectivity of products, in which the functional groups like N-, G-, -COOH, $-NH_2$, and -OH are used by which the adsorbed intermediates on the top layer of Cu- based electrocatalysts can be affected, the catalytic performance and selectivity for the catalyst was observed to be high as 90% when functional groups such

as N- and -OH is used was shown in the **(Fig.6)**. Different functional groups, when attached, showed different physical, chemical, and morphological properties (-COOH showed webbed-like morphology). The activity of the catalyst mainly lies in tuning the electronic properties by adding a metal to it, and here Ni is added with Cu to form $CuNi_2$@MWCNTs to increase the catalytic activity. FEs for H_2, CO, & formate as a result of applied voltage on each Cu_1Ni_2@ MWCNTs catalysts. We can infer that the functional categories lead to a powerful except for Cu_1Ni_2@G-MWCNT, HER inhibition catalysts. The selectivity of CO and HCOOH as reduction products by inducing functional groups to it has proven as an efficient electrocatalyst than pristine Cu- based electrocatalysts. This has proven to be a promising approach that can be induced on a larger scale. Agustin F. Perez-Cadenas and co-workers[47] report that as cathodes for the electro-reduction of CO_2 to hydrocarbons under non-ambient pressure condition, carbon xerogels doped with transition-metal compounds have been prepared as thin films. The metals Ni, Cu, and Fe are used for doping with xerogels, and the synthesis procedure includes preparation of the organic xerogel electrode with metal components and reference is also prepared using the same way and carbonized at 900 ˚C in N_2 atmosphere for 5 hours; these xerogel electrodes have the capability of efficiently converting CO_2 to C_1-C_4 products. Although the synthesis of both propane and ethane had been greater than with XCu, methane was the primary product that was found was shown in the **(Fig.6).** Throughout the 500 minutes of operation, neither propane nor C_4 hydrocarbons were found. After 270 minutes of reaction time, the overall molar production is measured and is comparable to that of XCu despite employing less metal (Fe) on the cathode but being easier to access. This result might be attributable to the potential difference in catalytic efficiency between Cu^0 and Fe^{2+}, but it is also essential to consider the substantially increased porosity and surface area of XFe, which may have contributed to a higher dopant dispersion. Different metals show different morphology as XNi and XFe have a microporous structure whereas XCu has comparably fewer micropores and surface area, so due to the morphological changes XNi and XFe have better activity and selectivity than XCu. This work does not provide information on faradic efficiencies and product selectivity, but it provides promising insight into using xerogel doped with metals as electrodes and electrocatalysts. Despite their varying chemical and textural characteristics, all of them can form hydrocarbons, albeit with varied product distributions. Tatsuya Shinagawa and co-workers[48] have reported Cu-S catalyst for electrochemical CO_2 reduction with selectivity towards formate production. The sulphur content is varied concerning Cu. It is observed that the increase in sulphur content favours the selectivity towards formate, i.e., FE > 45% and a current density of 2.5 mA cm^{-2} was shown in the **(Fig.6).** It is noteworthy that Cu-S catalyst selectivity yields formate, whereas the pristine Cu produces CO, alcohols, and hydrocarbons upon the electroreduction of CO_2. CO_2 is initially reduced to*OCHO or *COOH intermediates through one proton and electron transfer. The consequent reduction of *COOH produces *CO, which undergoes reduction leading to alcohols or hydrocarbons was shown in the **(Fig.6)**.

Furthermore, *OCHO is electrochemically reduced to HCOOH. Cu-S is exclusively selective to formate production because the sulphur contents alter the energy level requirements that correspond to the formation of the *OCHO intermediate. The binding energy between Cu-S and *OCHO is more vital than the pristine Cu due to the presence of positively charged Cu in the Cu-S. Overall, this study analyse the size dependence of the catalyst towards CO_2 conversion. Wen Ju and co-workers[49] have successfully investigated CO_2RR with porous carbon-containing M-N_X components, which are catalytically active and focus on CO product selectivity. The catalyst is prepared by a reaction of bipyridine-based coordinated polymers and metals such as Mn, Co, Ni, Fe, and Cu, the SEM images show the microporosity of the structures, which induces the activity and selectivity of the CO product was shown in the **(Fig.6)**. Here the Fe-N-C and Ni-N-C catalysts are compared with Au and Ag-based catalysts by examination of the CO faradic efficiencies and catalytic activity. Mn-N-C performance is plateauing, whereas the Ni-N-C catalyst significantly exceeds the performance of all other single-site catalysts and is increasing its CO generation rate at a highly high faradaic CO efficiency catalysing Au. The H_2 and CO accounts have the lowest faradaic efficiencies (FE) of all three main CO_2RR products after 60 minutes of electrolysis using the single-site catalysts for up to 95% of the transmitted charge. Compared to conventional Au catalysts, the Fe-N-C and Ni-N-C materials exhibit excellent CO efficiency at large and medium overpotentials, and their abundant ingredients on Earth make them desirable catalysts for use in the future. Industrial CO_2 consumption CO cathodes are intended for chlorine manufacturing as a counter electrode method. DFT studies and binding energies studies represent the M-NX components that are active. This shows insight into CO product selectivity, which is potentially dependent, and the M-NX components provide guidelines for an ideal catalyst for CO_2RR to highly selective products.

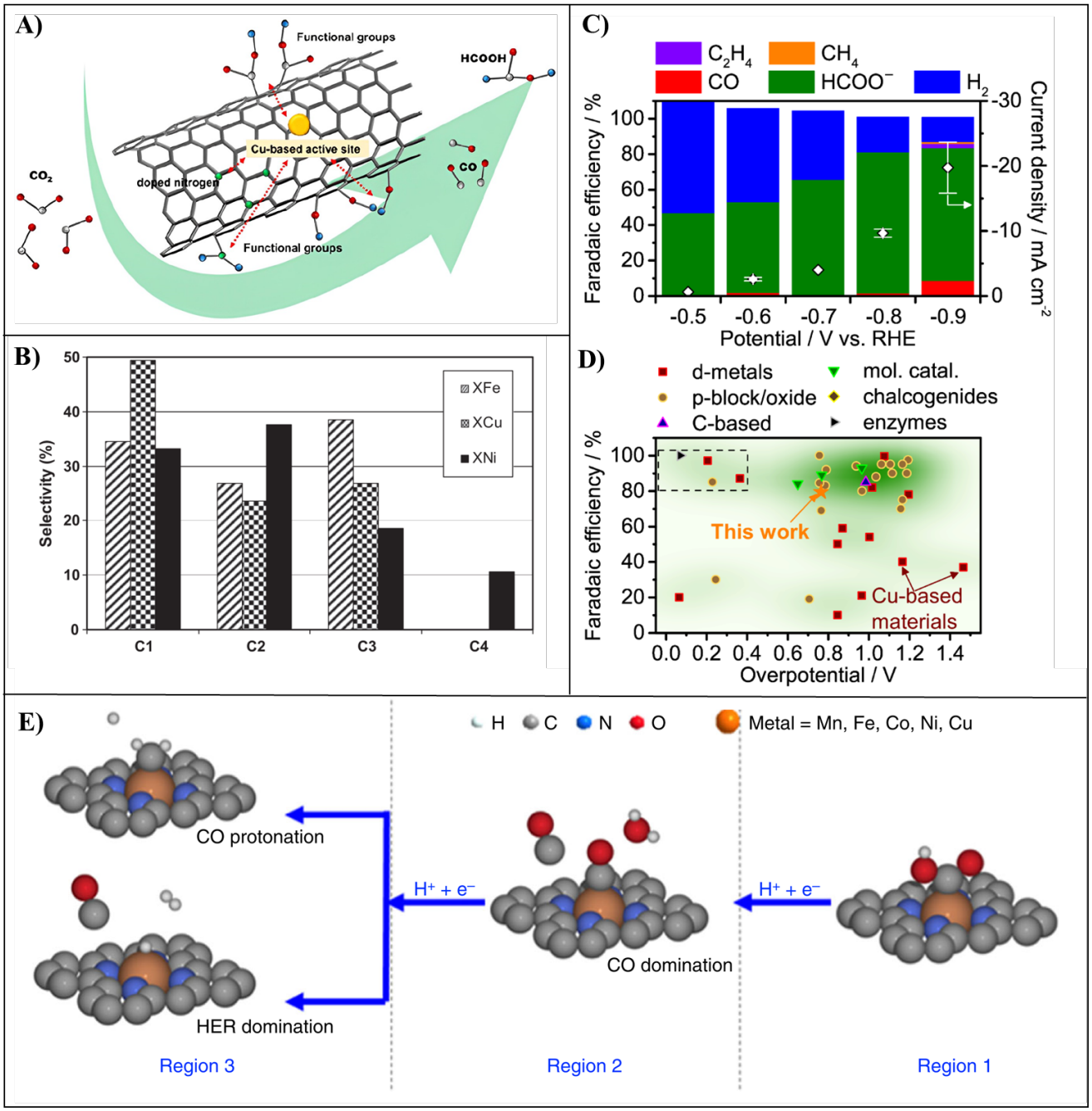

Fig.6 A) On a copper-based electrocatalyst supported by MWCNTs with various functional groups, CO_2 is reduced electrochemically. (Reproduced from ref [46] with consent from the American Chemical Society, copyright 2022) B) After 270 min of reaction time, the gas phase products that used metal-doped carbon xerogels for electrocatalysts were distributed (%) as a function of carbon selectivity. (Reproduced from ref [47] with consent from the Elsevier, copyright 2013). C) Faradic efficiency and total current density over the L-S sample as an estimate of applied potential. D) A literature-based faradic efficiency against overpotential for various groups of catalysts used in the CO_2RR process to produce formate. A dashed rectangle indicates the location of the standout performances, which are in the top left corner. There have

been reports of FE > 80% and 0.40 V) for non-scalable and/or inefficient systems. (Reproduced from ref [48] with consent from the American Chemical Society, copyright 2018). E) The reaction path B is divided into 3 possible areas, each having specific rate-determining mechanistic characteristics. (Reproduced from ref [49] with consent from the Nature Communication, copyright 2017).

Xiaolong Zhang and co-workers[50] reported electro-reduction of CO_2 using Cu nanoparticles immersed in N-doped carbon Cu@NC arrays for electrocatalytic CO_2 conversion reaction in DMF, here the arrays were fabricated from thermally decomposed tetracyanoquinodimethane which produces more active sites for catalytic reduction in N_2. This led to a 0.7 V positive shift in the onset potential, which resulted in dimethylformamide's (DMF) catalytic current density being an order of magnitude higher at a potential of -2.7 V vs. Fc/Fc^+ (Fc = ferrocene) (DMF). The distribution of the CO_2 reduction product can be adjusted by adjusting the amount of water in the DMF solvent. It was possible to produce 64% $HCOO^-$, 20% CO, and 13% H_2 under ideal circumstances (0.5 vol% water) was shown in the **(Fig.7)**. With only 0.5% decline in the steady-state catalytic current for 6 hours of electrolysis, the Cu@NC arrays demonstrated outstanding catalytic stability. The mechanism for CO_2 reduction Thus, as demonstrated in Eq. (3), $CO_2^{\bullet-}$ radical anions are first created on the catalyst's surface by reducing the adsorbed CO_2. The subsequent reaction between the $CO_2^{\bullet-}$ radical anion and CO_2 produces

$$CO.Cu_{(plate)} + TCNQ_{(sol)} \rightarrow CuTCNQ_{(film)} \quad (1)$$

$$CO_2 + * \rightarrow *CO_2 \quad (2)$$

$$*CO_2 + e^- \rightarrow *CO_2^{\cdot-} \quad (3)$$

$$*CO_2^{\cdot-} + CO_2 \rightarrow *C_2O_4^{\cdot-} \quad (4)$$

$$*C_2O_4^{\cdot-} + e^- \rightarrow *CO + CO_3^{2-} \quad (5)$$

$$*CO \rightarrow CO + * \quad (6)$$

According to Eq. (7)– (9), the $CO_2^{\bullet-}$ radical anion must protonate to create formate. A surplus water concentration of 0.03% in the DMF despite drying for two days over four molecular sieves suggests that water is the proton's most probable source.

$$*CO_2^{\cdot-} + H_2O \rightarrow *HCOO^{\cdot} + OH^- \quad (7)$$

$$*HCOO^{\cdot} + e^- \rightarrow *HCOO^- \quad (8)$$

$$*HCOO^- \rightarrow HCOO^- + * \quad (9)$$

The Cu@NC's three-dimensional (3D) array structure has been shown to be helpful in enhancing the catalytic activity while preserving long-term catalytic stability. Yan-Ling Qui and co-workers[51] have observed electro-reduction of CO_2 using Cu based Metal Organic Framework (MOF). This activity shows the selectivity and conversion efficiency of electro-reduction of CO_2 is low due to the low solubility of CO_2 in aqueous environment, to rectify this problem $Cu_3(BTC)_2$ Cu (MOF) as an agent to capture CO_2 was coated on carbon paper-based gas diffusion electrode (GDE). The outcomes demonstrate that the Cu-MOF,

in addition to GDE, modifies the ERC reaction's resultant selectivity and influence's reaction activity by adding Cu-MOF to GDE, a significant improvement in CH_4. For instance, under medium concentrations and higher overpotentials, the FEs for methane on GDEs with Cu-MOF contents in the 7.5–15 wt% range are 2–3 times higher than those on GDE-Blank was shown in the **(Fig.7)**. While, the FE of the competitive hydrogen production is decreased to 30%. This work opens the door for creating GDE for ERC with enhanced catalytic activity. Saudagar Dongare and co-workers[52] reported a nanostructured electrocatalyst containing N-doped graphene (NGN) decorated with Cu nanoparticles which possess enhanced electrocatalytic activity for the electro-reduction of CO_2. The size of Cu NPs is increased by the high loading of Cu (30wt %) due to particle agglomeration, according to characterization data. An electrochemical cell with two compartments was used for the ECR studies. Cu_2O/NGN exhibits the highest ECR activity for all evaluated electrocatalysts over the range of investigated potentials. This paper provides a straightforward method for efficiently converting CO_2 into useful compounds, and the findings are useful for creating alternative electrodes to reduce CO_2 electrochemically effectively. The findings imply that increasing the ECSA of engineered materials by altering the metal concentration on the NGN support leads to increased selectivity and activity for multi-carbon products. Maximizing Cu's availability by dimerizing the intermediate COOH*/CO* was hoped to increase the multi-carbon production rate. Additionally, increasing the C-C binding rate at lower overpotentials is anticipated to lead to an increased alcohol chain than ethanol/n-propanol. The liquid products result in an overall FE of 54% at -1.0 V (vs. RHE). The findings also indicate that adding Cu NPs to the NGN surface increased the electrode's electrical and structural characteristics, improving the catalyst's performance, as shown by potential-controlled electrocatalysis was shown in the **(Fig.6)**.

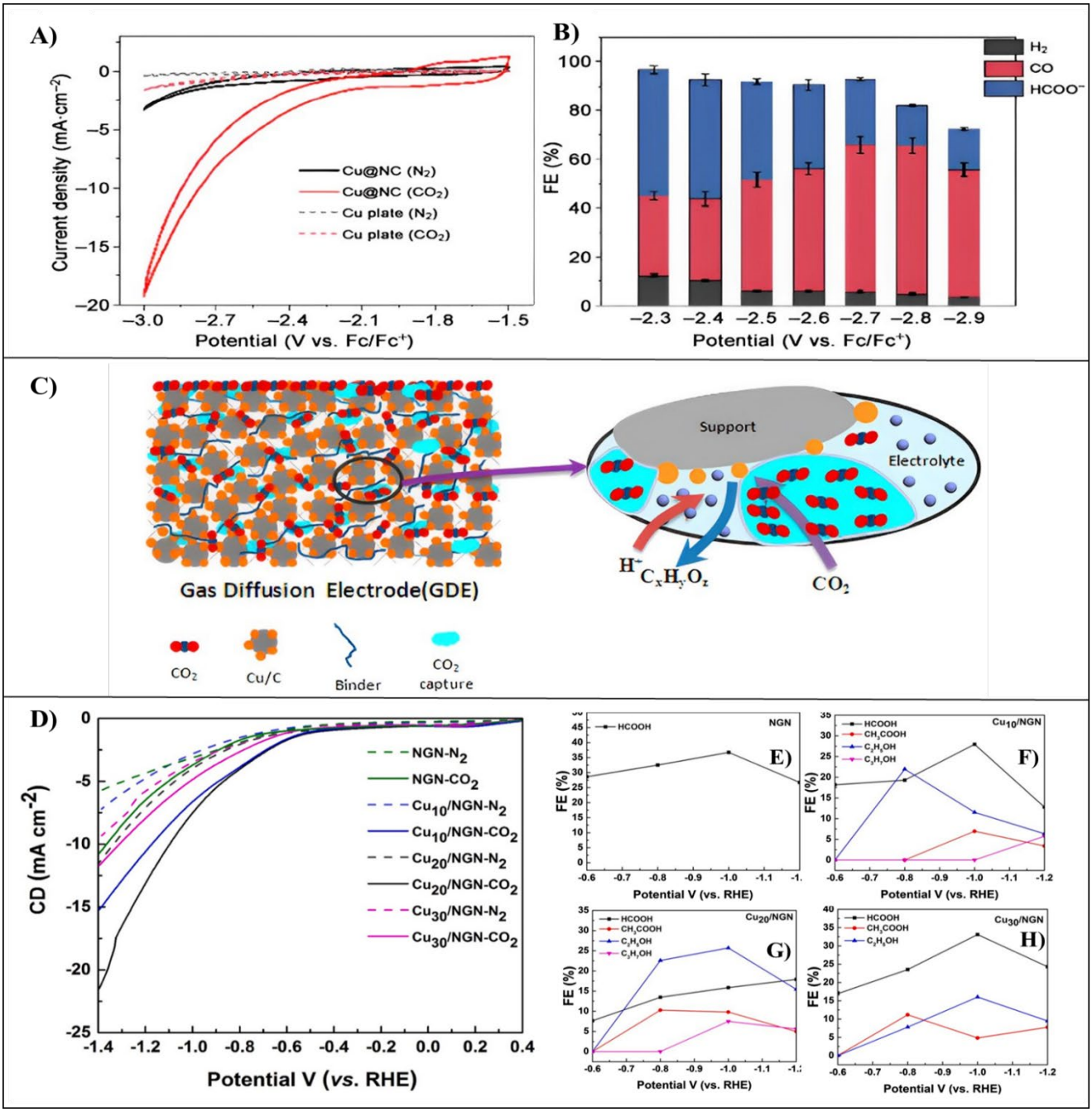

Fig.7 A) Cyclic voltammograms made with the polycrystalline Cu plate and Cu@NC B) Faradaic effectiveness for the generating of H_2, CO, and $HCOO^-$ is an expression of applied potential. (Reproduced from ref [50] with consent from the Springer Nature, copyright 2018). C) GDE structural schematic diagram showing the CO_2 capture agent $Cu_3(BTC)_2$. (Reproduced from ref [51] with consent from the American Chemical Society, copyright 2018). D) LSV curves of several electrocatalysts in aqueous solutions of 0.1 M $KHCO_3$ saturated with N_2 and CO_2. E-H) Faradaic Efficiency as a function of applied potential for liquid products with different catalyst. (Reproduced from ref [52] with consent from the Elsevier, copyright 2021).

Fangqi Yang and co-workers[53] have reported the electro-reduction of CO_2 to selective products which use stable single-atom electrocatalysts, which is attractive and testing, especially a cheaper way for scalable production. A simple, scalable method for creating a Cu single-atom catalyst with outstanding CO generation capabilities (Cu SAs/NC). HAADF-STEM and XANES investigations demonstrate the atomic dispersion of Cu-N_4 compounds. The synthesis of *COH required the most accessible energy, which was subsequently followed by *COCO (1.04 eV) & *CHO (0.87 eV). In contrary, the free energy of emitting *CO to create CO is an initiative. These outcomes align with the practical findings that CO_2 is highly selectively prone to produce CO. Since CO_2/*COOH's proton-linked electron transfer step had the highest upward energy barrier of 1.65 eV, it is hypothesized that this is the rate-determining step (RDS). Similarly, the crucial *OCHO intermediate's free energy changed during the production of HCOOH. The Cu SAs/NC catalyst offers a high CO FE of 92% at 0.7 V_{RHE} and excellent durability during 30 hours of stability electrolysis was shown in the **(Fig.8)**. This should be noted as an example of efficient production of CO using Cu single-atom electrocatalyst; through this method, 20 g samples can be produced in one batch through similar electrochemical performances. Xia Ma and co-workers[54] have reported MOF-derived carbon-supported Cu-In for the selective formation of CO by electroreduction of CO_2. The high conductivity, porous structure, and outstanding CO_2 adsorption make MOF-derived carbon materials a promising catalyst. CuIn/C was synthesized by pyrolyzing MOF precursors. The reduction of CO_2 is carried out in 0.1 M $KHCO_3$ electrolyte and the FE of products CO, HCOOH, and H_2 are determined. It is observed that on Cu/C, the FE of H_2 reaches higher than the FE of CO and HCOOH, which shows that Cu/C is more favourable for HER. In comparison, In/C shows FE of below 30% for H_2, which is due to high overpotential for hydrogen evolution, below 10% for CO over all applied potential, and FE of 5% at -0.7 V and 39% at -0.9 V. With an increase in concentration of Cu, increase in FE of CO is observed. $Cu_{90}In_{10}$/C shows high selectivity towards CO with FE of 85% at -0.75 V was shown in the **(Fig.8)**. Also, FE of less than 20% is observed for H_2. The reaction mechanism follows as where * indicates the active site on the catalyst's surface.

$$CO_2(aq) + e^- \rightarrow *CO_2^- (aq) \quad (10)$$

$$*CO_2^- (aq) + H^+ \rightarrow *COOH\ (aq) \quad (11)$$

$$*COOH\ (aq) + H^+ + e^- \rightarrow *CO\ (aq) + H_2O \quad (12)$$

$$*CO\ (aq) \rightarrow CO\ (g) \quad (13)$$

Although the surface area of $Cu_{90}In_{10}$/C is less than the In/C, which indicates that surface area is not the critical aspect of a catalyst for the CO_2 reduction reaction. Here, EIS shows that the $Cu_{90}In_{10}$/C poses the lowest charge transfer resistance and fastest electron transfer rate due to the smallest impedance radius,

which accelerates the reduction of CO_2 to CO. Xiao-Feng Qui and co-workers[55] have reported that MOF denoted as PcCu-Cu-O, that has a square planar CuO_4 nodes to convert CO_2 into C_2H_4 as the electrocatalyst. However, PcCu-Cu-O/CNT produces H_2 as the primary reduction product at all potential ranges (−1.0 to −1.6 V vs. RHE) and yielded no C_2H_4, which could be attributed to the enhanced catalytic activity for production of hydrogen by CNT. Notably, the performance of PcCu-Cu-O is observed as, FE(C_2H_4) of 25% with a FE of 50% and a current density of 7.3 mA cm2 at the potential of 1.2 V vs. RHE in 0.1 M $KHCO_3$ solution, PcCu-Cu-O exhibits significantly higher performance for electrocatalytic reduction of CO_2 to C_2H_4 than the molecular copper-phthalocyanine (FE of C_2H_4 = 25%). The characterisation analysis suggests that the improved electrocatalytic performance may be attributed to the synergistic effect between the CuPc unit and the CuO_4 unit, where the CO on the CO-producing site can efficiently migrate and dimerize with the *CO adsorbed on the production site of C_2H_4 (CuPc). According to the mechanistic study, such high performance may be attributed to the dual active sites' synergistic impact, which can lower the obstacle to energy in the C–C dimerization. Yeongdong Mun and co-workers[56] have developed Cu-Pd nanoparticles for electro conversion of CO_2 to CO. The selectivity of the reduction product is tuned by varying the composition of the Cu-Pd alloy. The production of CO is enhanced by the addition of Pd to Cu. Pd has relatively vital CO binding energy and low activity towards the production of H_2. At -0.7 V on Cu_{3an} Pd, an FE of 43% is observed for the formation of CO. At -0.9 V on CuPd, the formation of CO is superior to a maximum FE of 87% was shown in the **(Fig.8)**. This high selectivity towards gaseous products eases the separation for practical application. Cu_3Pd shows less selectivity towards CO t CuPd because of its broad size distribution of the nanoparticles. Thus, the larger size of the nanoparticle decreases the catalytic activity for the electroreduction of CO. For instance, FE of 54 and 65% are achieved for the formation of CO with Pd-5nm and Pd-3nm, respectively. In result, CuPd has the highest mass activity of 30 mA mg-1 for the formation of CO at -0.9 V. Here, CO_2 produce selectively produces CO rather than hydrocarbon because the limiting potential of the *CO protonation is much higher than pristine Cu. Thus, hydrocarbon production is suppressed. DFT displays the free change in energy of each fundamental step. First, the COOH* production phase is the potential determinant step (PDS) when we concentrate on the path for CO* formation that is significant to CO generation. In this stage, the limiting potentials for Cu (211) and CuPd (211) are respectively -0.41 V and -0.36 V. Although CuPd (211) has a lower limiting potential than Cu (211), the difference is only 0.1 eV, which could not be enough to account for the selection for CO generation. As a result, we also considered the following procedure, CO* protonation, which utilizes PDS for producing hydrocarbons. On Cu (211), HCO* formation is substantially more preferred to COH* formation. This work reports a high selectivity in the formation of CO for practical application was shown in the **(Fig.8)**.

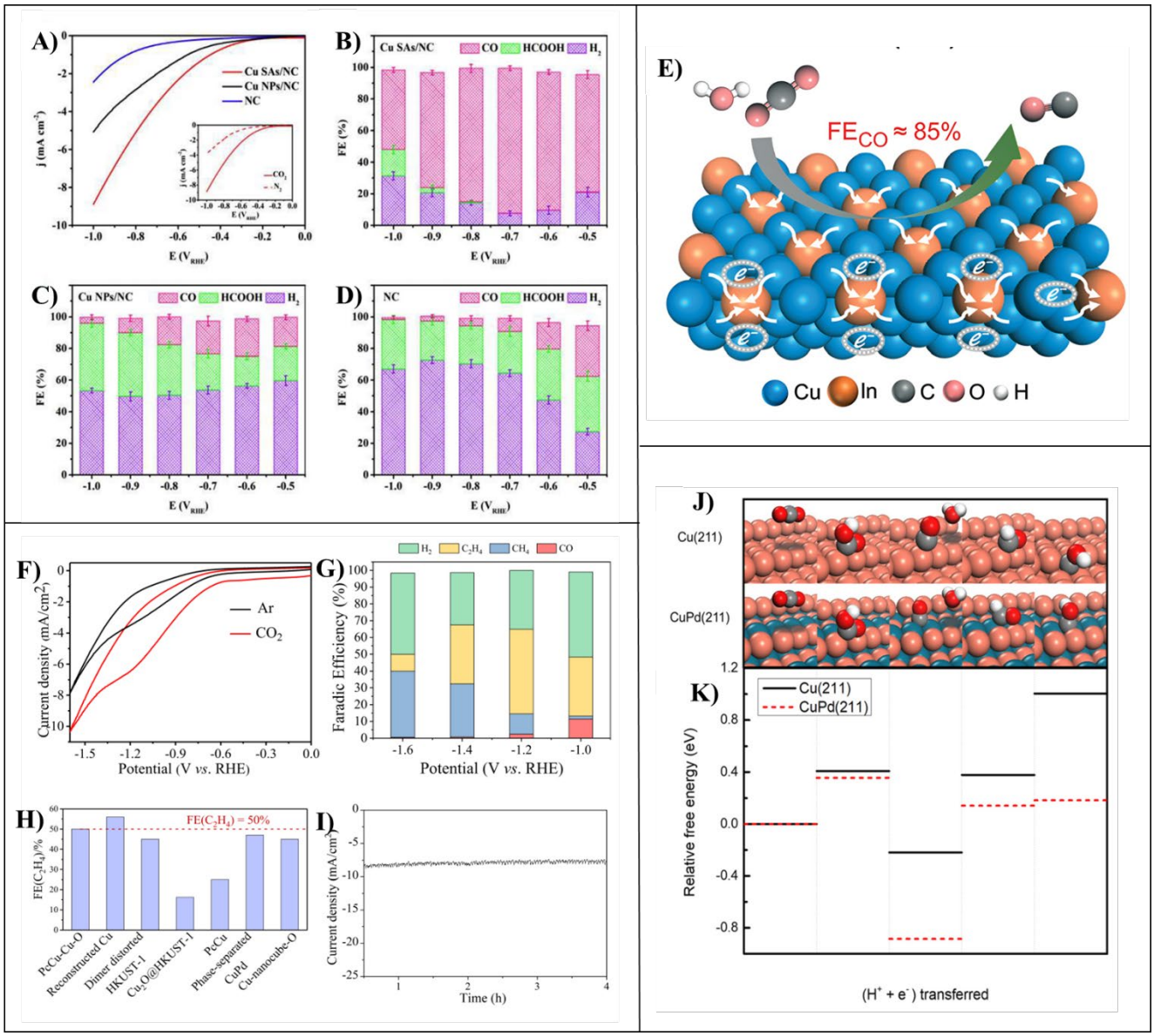

Fig.8 Faradaic Efficiency on A) Cu SAs/NC, B) Cu NPs/NC, C) Cu NPs/NC, and D) NC at various applied potentials. LSV curves in CO_2-saturated 0.1 M $KHCO_3$ electrolyte at 20 mV s1 (inset: LSV of Cu SAs/NC in N_2- and CO_2-saturated 0.1 M $KHCO_3$ electrolyte). (Reproduced from ref [53] with consent from the Elsevier, copyright 2020). E) A schematic illustration of the CO_2RR on $Cu_{90}In_{10}/C$. (Reproduced from ref [54] with consent from the Royal Society of Chemistry, copyright 2021). F) PcCu-Cu-O CV curves. G) FEs for PcCu-Cu-O for C_2H_4, CH_4, CO, and H_2 H) Comparisons between the FE(C_2H_4) produced between PcCu-Cu-O and other reported electrocatalysts. I) PcCu-Cu-O's resilience in the 1.2 V vs. RHE electrocatalysis potential. (Reproduced from ref [55] with consent from the American Chemical Society, copyright 2021). J) The reaction route that produces CO on the surfaces of Cu (211) and CuPd (211). H)

The CO_2RR free energy diagram on surfaces made of Cu (211) and CuPd (211). (Reproduced from ref [56] with consent from the Elsevier, copyright 2019).

Jian Xiang Wu and co-workers[57] have reported porphyrinic MOF nanosheets with paddle wheel clusters based on copper (II) for electrocatalytic conversion of CO_2. The cathode Cu-MOF nanosheets stand out for their substantial activity in producing formate, with a FE of 68.4% at 1.55 V vs. Ag/Ag^+ was shown in the **(Fig.9)**. At a voltage range of 1.40 V to 1.65 V, the same catalyst generates formate and C-C coupling resulting in product acetate, with the total liquid product FE ranging from 38.8% to 85.2%. The cathode reformation of Cu-MOF nanosheets is intimately related to their high selectivity and activity. The characterisation findings show that Cu (II) carboxylate nodes may change to CuO, Cu_2O, and Cu_4O_3, which significantly convert CO_2 to formate and acetate with synergistic enhancement from the porphyrin-Cu (II) complex. This activity results in a chance for the logical construction of high-performance Cu catalysts from pre-designed MOFs. Yong Zhao and co-workers[58] have developed a CuO nanowire decorated with tin nanoparticles to form CO by aqueous CO_2 conversion efficiently. Cu-Sn nanowire electrode is made by immersing Cu foil into Sn electroless plating bath for the deposition of Sn nanoparticles. Here, the deposition time plays a significant time in the activity of CO_2 reduction. The pristine Cu nanowire has reduced the CO_2 to H_2, C_1, and C_2 products, whereas the Cu-Sn nanowire electrode has only produced H_2 and C_1 products. This demonstrates the selectivity for C_1 products in Cu-Sn nanowire electrodes. A lower FE < 20% for CO and higher FE > 60% for H_2 is observed in the pristine Cu nanowire electrode was shown in the **(Fig.9)**. In contrast, the Cu-Sn nanowire electrode showed higher selectivity for CO (FE 80%) and suppressed the evolution of H_2 was shown in the **(Fig.9)**. By increasing the deposition time of Sn, the FE of H_2 and C_1 products are increased. The FE of CO is increased in deposition time of 10s, and a decrease in FE is observed with prolonged deposition time. These results imply that the CO_2 to CO conversion is due to the synergistic interaction between the Cu nanowires and Sn nanoparticles. The Cu-Sn electrode shows high selectivity for CO due to the multifold sites of the Sn atom on the surface of pristine Cu, which suppress the adsorption of H_2 and Favors the adsorption of CO. Further, the FE of CO is increased to 90% by introducing Au to the Cu-Sn electrode. This study paves a new way for large-scale conversion of CO_2 by Cu-based electrodes was shown in the **(Fig.9)**. Xin Guo and co-workers[59] have demonstrated the composition-dependent electroreduction of CO_2 activity of CuPt nanocrystal catalyst. Here, the CuPt catalyst is dominated by HER rather than CO_2 reduction. The HER is suppressed by applying a potential lower than -1.1 V. Therefore, the highest FE of 21% is obtained to form CH_4 with CuPt-4# catalyst. A similar study is carried out with polycrystalline Cu and Cu nanoparticles; these show FE of 4 and 1%, respectively, for methane formation. This indicates that CuPt is highly selective to the production of CH_4

than Cu nanoparticles. The Density Functional Theory (DFT) results suggest that the production of CH_4 from the electro conversion of CO_2 is due to the protonation of CO* to give HCO*.

$$CO* + H^+ + e^- \rightarrow HCO* \quad (14)$$

Initially, the CO_2 is reduced to CO and further protonated to HCO. The presence of Pt, which has a high affinity towards the proton, thus, facilitates the formation of CH_4. The production of H_2 during CO_2 reduction is due to the strong interaction between Pt and CO*, which segregates the Pt that attributes to HER over CO_2 reduction. The CuPt (3:1) shows the highest activity. However, a further increase in the Cu content leads to a higher density of CO*, which lowers adsorbed proton; thus, methane formation may decrease was shown in the **(Fig.9)**. This work brings up a new strategy for the electroreduction of CO_2 to CH_4 by the compositional effect of nanocrystals. Nianjun Yang and co-workers[60] observed that the entire surface of the diamond electrode is enclosed in copper nanoparticles was shown in the **(Fig.9)**. Both their size and distribution are constant. To be clear, homogenous deposition, a wet-chemical process, was used to create copper nanoparticles. These copper nanoparticles have a density of around 4.6 (±0.5) 10^{10} cm^{-2}, resulting in an 81(±1.0) % of the surface being covered. By electrochemical overgrowth, Cu nanoparticles up to 1.0 m in diameter were attempted.CO_2 electro-conversion on a diamond electrode which is enriched by Cu nanoparticles, when using a solution of water and ionic liquid ([H_2O] = 10 M), CO_2 conversion begins at 0.1 V compared to a Standard Hydrogen Electrode (SHE). At a potential of 1.3 V versus SHE, the current density for CO_2 reduction reaches 5.1 ± 0.1 mA cm^2. According to the Gas Chromatography (GC) and High-Performance Liquid Chromatography (HPLC) product analysis, formic acid and formaldehyde are the two major products. Other byproducts, including H_2, CH_4, and C_2H_4, were also discovered. Formic acids byproducts could come from the radicals of CO_2 and anions reacting with water. Nonaqueous solutions for CO_2 reduction following CO_2 saturation of BMIM-PF_6, a visible wide cathodic shoulder is observed at around -2.0 V vs. SHE, comparable to other RTILs.8,13 In BMIM-PF_6, the cathodic waveform at 2.0 V vs SHE shows that $CO_2^{\bullet-}$ anion radicals have formed. With the help of adsorbed CO_2, these free radicals are further converted, resulting in the production of products in solutions connected to $C_2O_4^{2-}$. The electrode system also has a long lifetime and is stable. Therefore, it holds promise for use in bulk manufacturing of chemicals and fuels using CO_2 as a primary source. Juqin Zeng and co-workers have employed Cu-Zn catalyst composed of monocrystalline ZnO nanoparticles and polycrystalline Cu particles for electroreduction of CO_2. Here, microwave-assisted synthesis is carried out, which is a sustainable process compared to hydrothermal method and pyrolysis. Also, this technique is favorable for the scalable production of the catalyst by altering the precursor quantities and reactor system. The results show that the [61]Cu electrode at a potential ranging from -0.8 V to -1.1 V produces H_2, and it shows a FE of 9% at -0.9 V and a constant of 8% at the studied potential range for CO and HCOOH,

respectively. On the other hand, the ZnO electrode shows a high selectivity towards the formation of CO with a FE of 74%. It has been observed that with the increase in ZnO content on the electrode, the FE of CO also rises. The increase in the surface area of ZnO leads to a pathway toward more selective reaction sites for the formation of CO. Also, it is noteworthy that a further increase in Zn decreases the selectivity towards CO. For instance, the FE of CuZn0.4 is higher than CuZn0.5. The CuZn0.4 electrode maintains a partial density of 4.3 mA cm^{-2} and retains FE of 70% and 28% for forming CO and H_2, respectively, at stability for 4hrs. This work shows the need of balancing ZnO and Cu contents and proposes a way to develop low-cost catalysts and environmentally friendly fabrication methods.

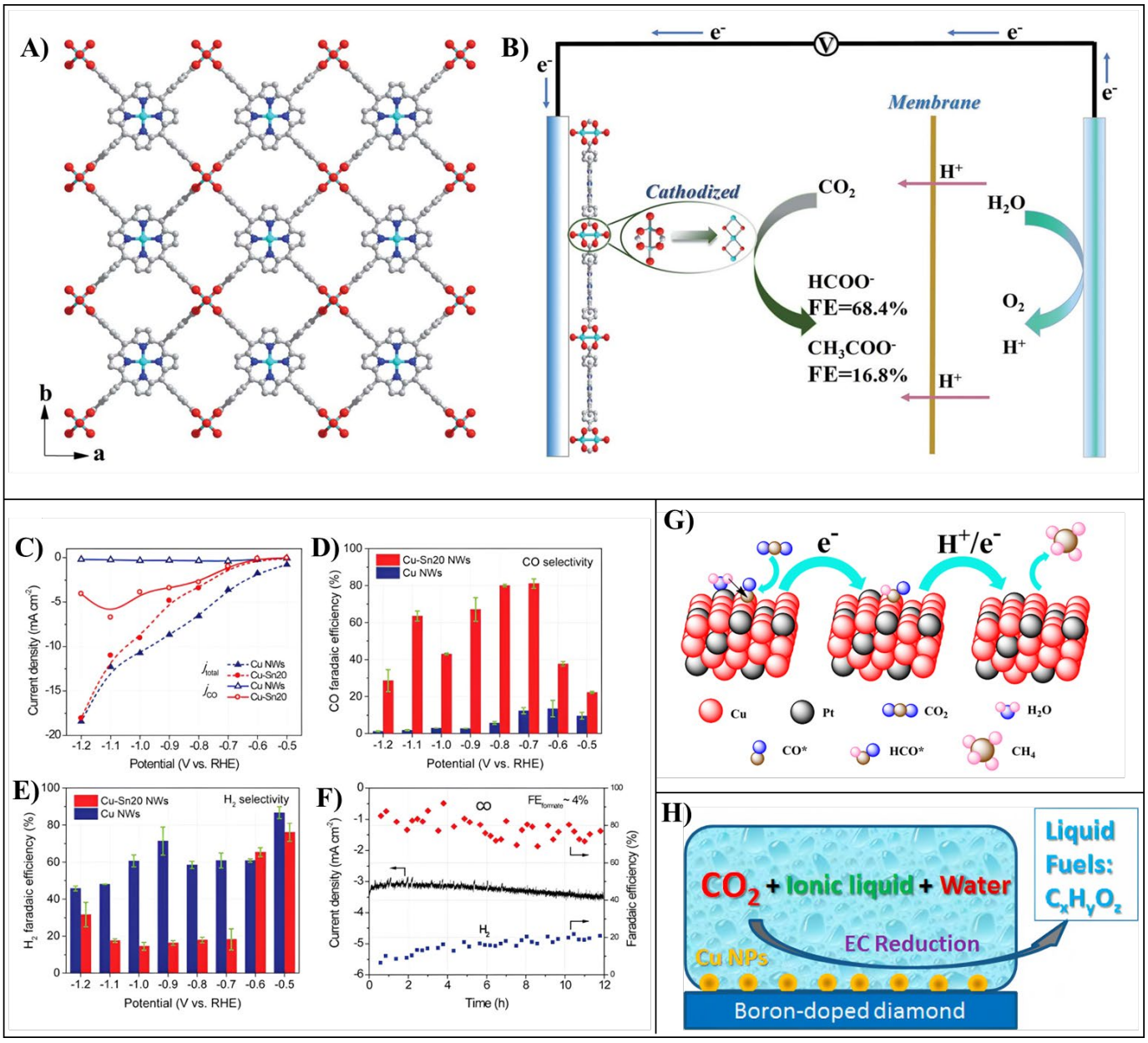

Fig.9 A) Cu_2(CuTCPP) nanosheets crystal structure is along the c axis B) CO_2 electro-reduction setup with Cu_2(CuTCPP) nanosheets acting as the catalyst, red denotes oxygen, blue nitrogen, grey carbon, and cyan copper. (Reproduced from ref [54] with consent from the Royal Society of Chemistry, copyright 2018). C) Lines to direct the eye's attention to the overall current densities and CO limited current densities for fixed CO_2 electro reduction using Cu NWs and Cu-Sn20 NWs at different potentials in 0.1 M $KHCO_3$. D- E) a contrast between the FE of CO and H_2 between Cu-Sn20 NWs and Cu-NWs at various potentials F) Cu-Sn20 catalyst's long-term stability was tested for 12 hours at -0.8 V (versus RHE) in CO_2-saturated 0.1 M solution of $KHCO_3$. Based on D) and E), the error bars show one standard deviation in three separate samples were measured. (Reproduced from ref [58] with consent from the Royal Society of Chemistry, copyright 2016.) G) At the Cu-Pt (3:1) NCs catalyst, a hypothesized mechanism exhibiting the phases of CO_2 electroreduction and the CH_4 production takes place. (Reproduced from ref [59] with consent from the Royal Society of Chemistry, copyright 2015). H) Copper nanoparticle-decorated diamond for electrochemical carbon dioxide reduction. (Reproduced from ref [60] with consent from the American Chemical Society, copyright 2013)

4.2 Copper-based catalyst for C_2 and C_{2+} product:

The progress of cooper-based catalyst for the conversion of CO_2 to C_2 and C_{2+} products follow as, Kun Zhao and co-workers have successfully synthesized an efficient electrocatalyst with a single copper atom anchored to nano porous carbon (Cu-SA/NPC); at a low overpotential, the Cu-SA/NPC converts CO_2 to multi carbon products, with acetone standing as the primary outcome. The oxidation state is Cu^{2+} is very adept for the electrochemical reduction of carbon dioxide. This catalyst exhibits increased production of multi-carbon products like CH_3OH, CH_3COOH, C_2H_5OH, and CH_3COCH_3. The mechanism and active sites show that the Cu^{2+} species should be atomically dispersed and was fourfold associated with N atoms in the Cu-SA/NPC, with respect to the characterisation data. Here, two kind of catalyst models were developed with a single Cu atom doped into a graphitic sheet that had four pyridine N atoms (Cu-pyridinic-N4 site) with four pyrrole N atoms as coordination environments (Site of Cu-pyrrolic-N4). The total process of generating CH_3COCH_3 from CO_2 reduction has a negative free energy change, indicating that the Cu-SA/NPC catalyst, CH_3COCH_3 had favourable thermodynamic properties. When a -0.36 V potential was applied, the fundamental CO_2 reduction steps to CH_3COCH_3 proceeded more thermodynamically downwards, but when a potential of 0 V was applied, indicating that the electroreduction environment made the synthesis of CH_3COCH_3 from CO_2 reduction more favourable was shown in the **(Fig.10)**. In the present DFT analysis, the ΔG value determined at -0.36 V for COOH* forming on Cu-pyrrolic-N_4 was 1.06 eV, is lesser than Cu-pyridinic-N_4 (1.30 eV) and indicated that CO_2 reduction might be more accessible on the Cu-pyrrolic-N_4 site of Cu-SA/NPC. Acetone is a significant outcome with a maximum faradic efficiency

of 36.7% at a production rate of 336.1 μg h^{-1}. The particular Cu-pyrrolic-N_4 active sites corresponds to the unique selectivity towards formation of acetone through CO_2 conversion on the Cu-SA/NPC catalyst by stabilizing the reaction intermediates that contribute to acetone production and facilitating the C-C association reactions due to the Cu-N synergy.[62] Pengtang Wang and co-workers have reported that a silver-modified copper oxide catalyst (dCu_2O/Ag) demonstrates a considerable energy efficiency for enhanced EtOH generation of 22.3% and a notable faradaic efficiency of 40.8% was shown in the **(Fig.10)**. Importantly, it converts CO_2 to ethanol while operating at high current levels with a limited current density of 326.4 mA cm^2 at a potential difference of 0.87 V from reversible hydrogen among the described Cu-based catalysts; the electrode will be highly significant. The ideal dCu_2O/Ag2.3% ratio favors the reduction of CO_2 to C_2H_4 and CO, respectively, in contrary to Cu_2O and Au-modified Cu_2O derivatives had an asymmetric C-C connection that stabilized reaction intervening products for increased EtOH generation at a high current density. The *CO binding capacity creates a mixed adsorption arrangement that increases the generation of ethanol (EtOH) and causes asymmetric C-C coupling to stabilize EtOH. For EtOH synthesis in a flow cell, an optimized dCu_2O/Ag2.3% demonstrates a FE of 40.8% and EEHF of 22.3%, as well as increased EtOH limited current density of 326.4 mA cm^2 at 0.89 (With an iR adjustment of 85%) V RHE. The enhanced EtOH selectivity is a result of the moderately coordinated surface and optimal oxidation state of the copper, which produce mixed $*CO^{bridge}$ and $*CO^{atop}$ topologies for asymmetric C-C coupling to stabilize the EtOH intermediate, according to in situ ATR-IRAS spectroscopy.[63] Cheng and co-workers have successfully synthesized a Cu- based catalyst that is modified by carbon and nitrogen (Cu-NC), which supports as an efficient electrocatalyst for CO_2RR, the catalyst used is MOF-derived copper @nitrogen doped carbon (Cu-NC); the catalyst is constructed by calcination of N-containing benzimidazole (BEN) modified with Cu-BTC. As a result, a modified MOF has been synthesized, BEN-Cu-BTC. Different samples have been synthesized at different temperatures, targeting different C_2 product selectivity. The results show that the C_2 product conversion is comparatively high for pyrrolic-N at 400°C, whereas the activity for oxidised-N and graphite-N is higher in HER, and the carbon dioxide reduction reaction is low. The abundant CO_2 is produced by the high pyrrolic-N and Cu-N doped levels in carbon supports the adsorption sites and also promotes carbon-carbon coupling processes on the surface of Cu, displaying an outstanding degree of selectivity for the production of ethylene and ethanol as products was shown in the **(Fig.10)**. The faradic efficiencies and the reaction rates for reduced species such as ethylene and ethanol at -1.01V (vs. RHE) are reported as $r_{ethylene}$= 5.38 μmol.m^{-2}, $r_{ethanol}$= 8.83 μmol.m^{-2} with a FE of 11.2% and 18.4% respectively. This study also demonstrates that the catalytic efficiency of the MOF-derived Cu-NC catalyst can be increased through the changes in the N-types, which leads to a new class of electrocatalysts used in efficiently reducing CO_2. [64]

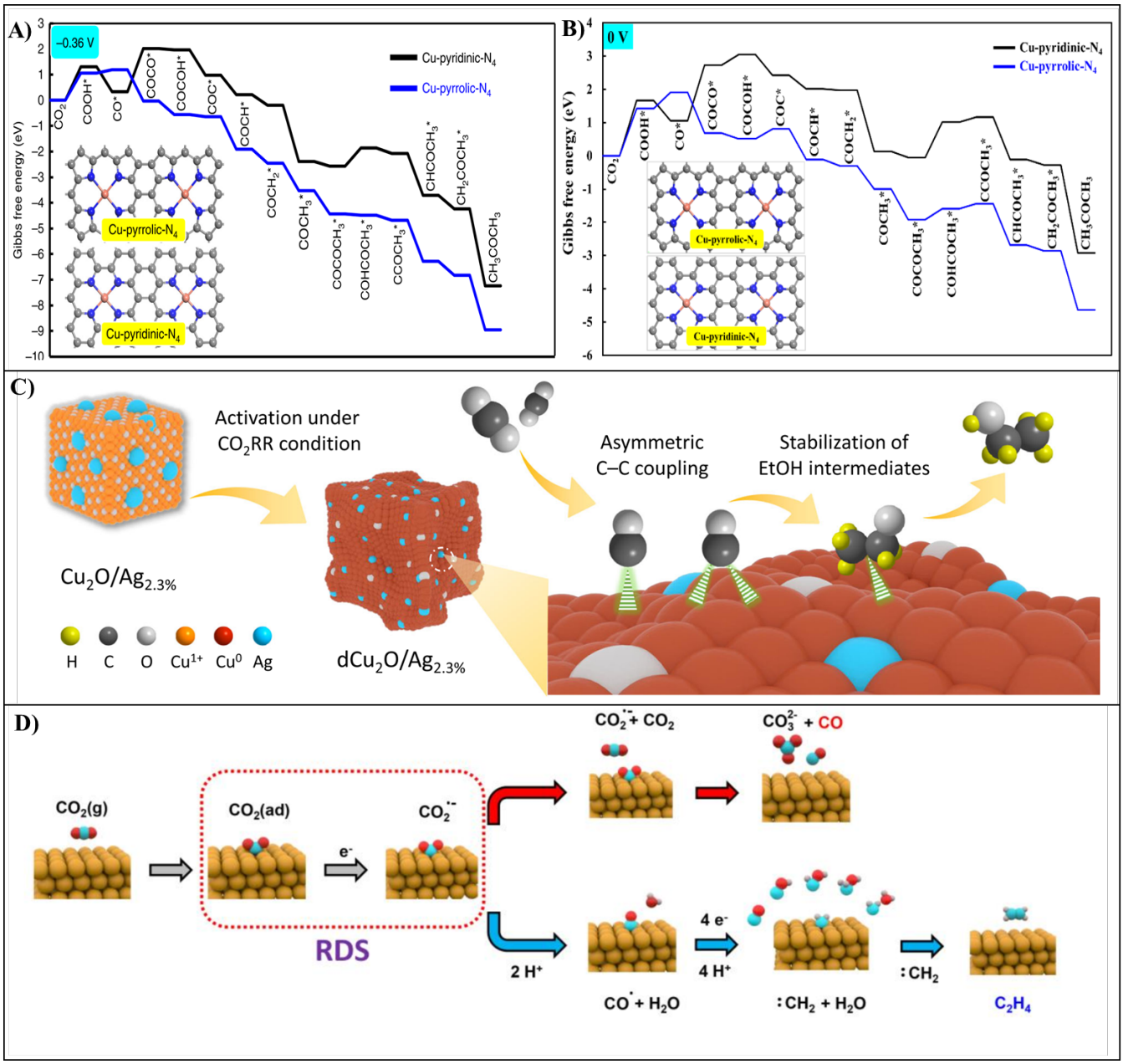

Fig.10 A) Free energy plots calculated for the CO_2 reduction to CH_3COCH_3 on the Cu-SA/NPC's Cu-pyridinic-N_4 and Cu-pyrrolic-N_4 sites B) Free energy calculated at 0 V for the reduction of CO_2 to CH_3COCH_3 at the Cu-SA/NPC's Cu-pyridinic-N_4 and Cu-pyrrolic-N_4 sites. (Reproduced from ref [62] with consent from the Nature Communication, copyright 2020). C) Diagram showing enhanced EtOH production over $dCu_2O/Ag_{2.3\%}$. (Reproduced from ref [63] with consent from the Nature Communication, copyright 2022). D) The CH_2-CH_2 dimerization pathways to C_2H_4 (blue) and the CO production pathways (red) on the Cu surface. (Reproduced from ref. [65] with consent from the Royal Society of Chemistry, copyright 2019).

Dilan Karapinar and co-workers reported a novel CO_2RR catalyst that focuses on ethylene as the reduction

product. This efficient copper nitrogen-doped carbon material (Cu-N-C) is exclusively prepared by the pyrolytic method, and it contains atomically distributed single copper atoms which possess multiple oxidation states +1 and +2, in a nitrogen-doped conductive carbon matrix with a CuN_4 coordination. The morphology of the catalyst synthesized does not show any specific morphology before and after the activation of the catalyst. The activity of the species is due to the reduction of the CuN_4 sites into metallic Cu nanoparticles, as shown in the X-ray Absorption Spectroscopy (XAS) analysis. The main reaction products were determined to be CO and H_2, with the FY for CO, reaching outmost at various potentials depending on the electrolyte (47% for $LiHCO_3$ at -0.8 V, 58% for $NaHCO_3$, 64% for $KHCO_3$, and 74% for $CsHCO_3$ at -0.7 V) was shown in the **(Fig.11)**. Using 13C-labeled CO_2 (-1.2 V, 2.5 mL/min CO_2), we performed the catalytic test to verify that CO_2 served as the ethanol carbon source as a liquid phase according to the description 1H and 13C NMR data. Ethanol heated up to 13℃ labeling after 1 hour of electrolysis confirmed that it comes from CO_2 reduction. The bigger cations once more favored ethanol synthesis under ideal conditions (-1.2 V, 2.5 mL/min CO_2), with FY(EtOH) rising in the following order: Li^+ (2%) Na^+ (5%) K^+ (16%) Cs^+ (43%) was shown in the **(Fig.11)**. The reduction of CO to products to ethylene or ethanol is produced with a faradic efficiency of 80%, and the conversion of CO_2 to ethylene produces a faradic efficiency of 55% under the influence of 0.1 M $CsHCO_3$ with a potential of -1.2V vs. RHE, the reversible nature of the reversible hydrogen electrode surprisingly leads to the reversibility of the catalyst after the conversion.[66] Aravind V Rayer and co-workers have reported electrochemical CO_2 to isopropanol by employing a novel carbonized copper MOF-derived electrodes; however, copper is an efficient electrocatalyst for the production of products from CO_2, and it also remains a challenge for producing low-cost, stable, and product-selective catalyst, the findings concerning the potential of electrocatalyst derived from carbonized MOF for electrochemical conversion of CO_2. Two commercially available copper-decorated MOFs, namely, HKUST-1 and PCN-62, were taken, and metallic nickel and copper supports as inks were applied and pyrolyzed at varying temperatures of 400–800 °C. First, CO_2 is extracted and purified from its source, such as cement plants, directly captured from the air or flue gases from power plants. The goal is to eliminate pollutants (SO_2, NO_X) and undesirable components (O_2) and concentrate the CO_2 into > 95 vol%. In addition to the water used for processing and recycled electrolyte, the purified CO_2 is sent to the basic water-based CO_2 reduction electrolyzer premixed with recycled CO_2. The electrolyzer receives off-grid, sustainable electrical power to divide the water and reduce CO_2 simultaneously. Most significantly, Gas Chromatography-Flame Ionization Detector (GC-FID) analysis confirmed the creation of isopropanol, a product that had not, to the best of our knowledge, been previously reported.[67]

Table.2 The CO_2 reduction reaction (CO_2RR) catalytic behavior of the studied electrocatalysts.

Electrocatalyst	FE_{HER} (%)	FE_{CO2RR}	$FE_{isopropanol}/FE_{other}$
Cu-Mesh	56.70	43.30	1.50
Cu-Foil	62.90	37.10	1.60
Cu-PCN62@800℃	91.80	8.20	1.90
Cu-PCN62@600℃	92.70	7.30	2.00
Ni-PCN62@800℃	70.90	29.1	0.40
Cu-HKUST-1@600℃	77.50	22.5	2.70
Ni-HKUST-1@600℃	24.90	75.1	0.10
Ni-HKUST-1@400℃	92.10	7.90	1.90

The superior electrocatalyst showed isopropanol faradaic efficiency (FE) of over 72% among all the carbon products was shown in the **(Fig.11)**. The suggested electrochemical CO_2 reduction method needed to operate at a target cell operating voltage for a preliminary techno-economic study to show that it could be economically implemented.

Jing Yuan and co-workers reported an effective electrochemical conversion of CO_2 to ethanol on Cu nanoparticles supported N-doped graphene oxide catalyst. The electrochemical conversion of CO_2 to C_2H_5OH is enhanced by modifying the Cu nanoparticles with pyridoxine. As strong electrocatalysts, graphene oxide sheets (GO-VB_6-Cu) are used. GO-VB_6-Cu-2 catalyst was successfully used to convert CO_2 to C_2H_5OH in 0.1 M $KHCO_3$ solution at an overpotential of just 0.140 V. At a voltage of 0.250 V vs. RHE, the most outstanding Faradaic efficiency for the production of ethanol of 56.3% was achieved. After almost 24 hours of continuous use, the resulting nanocomposite showed no deterioration, demonstrating the electrode's notable stability. Electrocatalytic active surface area, improved CO_2 adsorption, and reduced electron transfer resistance are factors to the remarkable response toward CO_2 reduction that was attained here. A potential mechanism supported by electrochemical kinetics data for GO-VB_6-Cu comprises a reversible electron transport to CO_2 to form CO_2*, followed by a series of proton-electron transfers to produce CO* was shown in the **(Fig.11)**. Further dimerization of CO* results in the formation of OC-CO*, which could represent the crucial rate-determining step, and ethanol is produced by protonating and further reducing the obtained OC-CO*. **(Fig.11)** illustrates a potential CO_2 conversion method on GO-VB_6-Cu. The total amount of Cu in the GO-VB_6-Cu catalyst affected CO_2 reduction efficiency. The efficiency of several GO-VB_6-Cu catalysts in the potential range of -0.050 V to -0.450 V vs. RHE was shown in the **(Fig.11)**. As anticipated, the GO-VB_6-Cu catalysts with varying Cu content showed various electrocatalytic activity for C_2H_5OH synthesis. As the potential switched to the negative position, the FEs of C_2H_5OH production on different GO-VB_6-Cu catalysts displayed volcanic-like tendencies.[68] Zhen-Hua Zhao and

co-workers have reported Cu (111) @Cu-THQ for electrochemical conversion of CO_2. The CuO_4 nodes of 2D conductive Cu-MOF exhibit outstanding performance in converting CO_2 to CO with 91% FE and ca. 20.82 s^{-1} of turnover frequency. This high conductivity of Cu-THQ accelerates the electron transfer process and eases the electro-reduction of CO_2 to C_2H_4. The Cu (111) nanoparticles were orderly deposited on the surface of Cu-THQ by in situ electrochemical synthesis. In general, Cu (111) facet favors converting CO_2 to CH_4, but by optimizing the electrolyte and catalyst morphology, Cu (111) facet may selectively produce C_2H_4. A tandem catalytic mechanism achieves a high conversion efficiency of CO_2 to ethylene by incorporating the catalytic active sites of Cu (111) and Cu-THQ. FE(CH_4) was insignificant at -1.0 V, but FE(C_2H_4) was 37.4 ± 2.4% have greater efficiency. The current density (j) was 8.2 mA $cm^{-2,}$ and FE(C_2H_4) was enhanced to 44.2 ± 3.4% when the cathodic potential was reduced to -1.2 V. When the opportunity was greater, FE(C_2H_4) potential was slightly decreased to -1.4 V and 42.2 ± 1.4%, but a large increase in the j value to 14.3 mA cm^{-2}. According to DFT, it is clear that the CuO_4 site of Cu-THQ is the preferred active site for producing the *CO intermediate. Additionally, the energy hurdle for CO desorption on the CuO_4 site is much lower (0.236 eV) than it is for the *CO → *CHO pathways (0.761 eV), implying the fact that *CO on the CuO_4 site is more likely to desorb instead of be reduced further to a *CHO intermediate was shown in the **(Fig.11)**.[69]

Xinyi Tan and co-workers have reported the tailored multifunction coupled Cu-MOF by time-controlled conversion of Cu_2O to Cu_2O@Cu-MOF. The weak CO_2 absorbability on the Cu_2O surface compared to the hydrated ions for the hydrogen may cause the inadequate CO_2 electro-reduction efficiency of Cu_2O response to hydrogen production. The Cu-MOF produces only 49.7% hydrocarbon FE and a poor CH_4/C_2H_4 ratio of 2.86:1. To put it another way, Cu_2O@Cu-MOF displays the most remarkable affinities for CH_4 and all hydrocarbons FE. Long-term electrolysis is also used to assess the catalyst's stability for the Cu_2O@Cu-MOF catalyst. The converted electrocatalyst is time dependent and has sufficient surface area for CO_2 adsorption and has more active sites for the excellent activity for electrolysis based on the MOF surface of Cu_2O as well as charge transfer derived from Cu_2O core compared with Cu-MOF. These unique traits ultimately result in an impressive performance towards hydrocarbons, with a high hydrocarbon FE of 79.4%, specifically, the FE of CH_4 is as high as 63.2% (at 1.71 V), strong adsorption ability, and large surface area and significantly more exposed active sites, this work proposes an effective technique to build MOFs for energy related applications. [70]

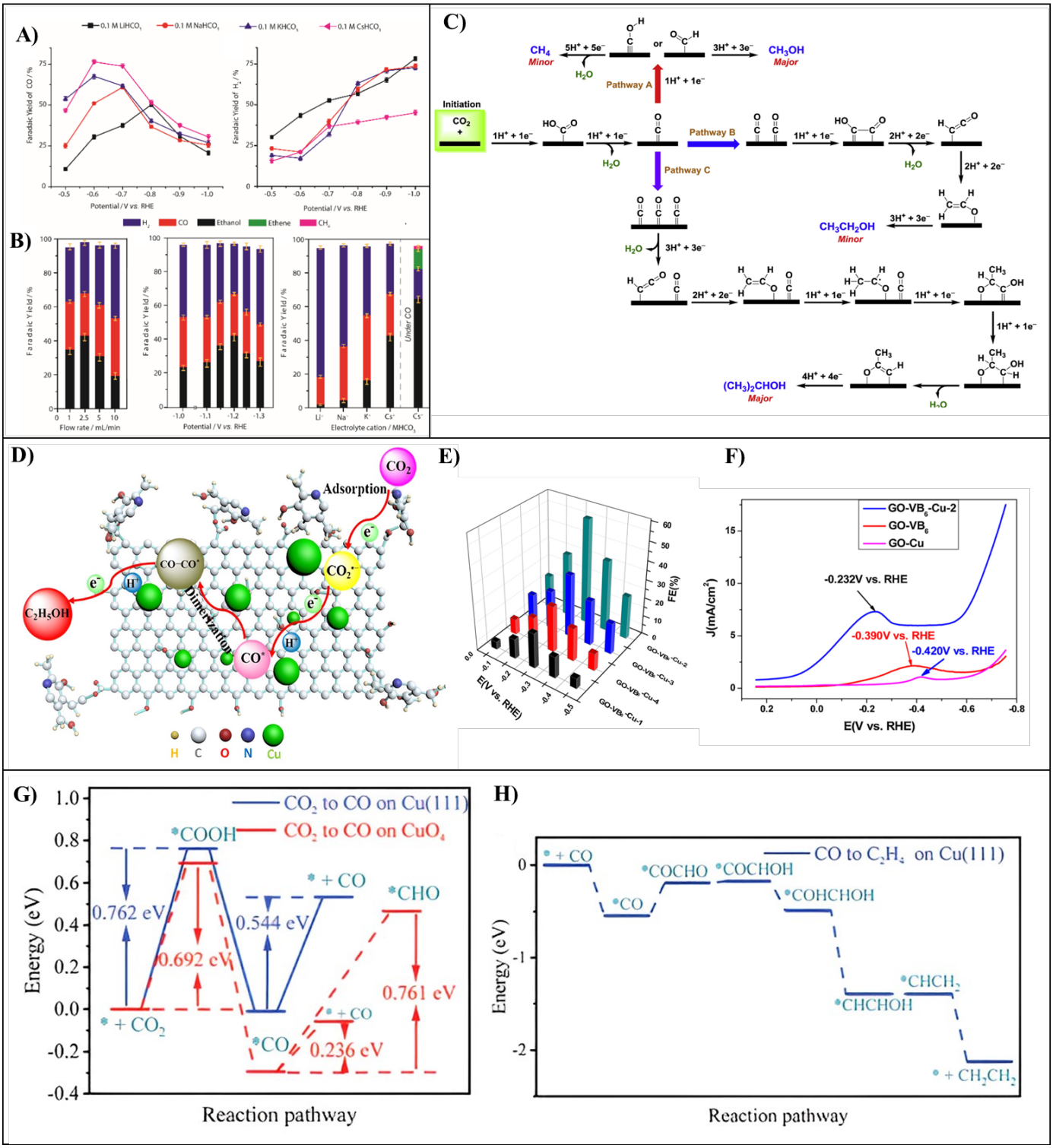

Fig.11 A) Faradic Yield of CO and H_2. B) FYs for CO_2RR under flow conditions at -1.2 V vs. RHE at various applied potentials during CPE at 2.5 mL/min CO_2 flow rate were employing different electrolyte cations at -1.2 V vs. RHE and 2.5 mL/min flow rate. (Reproduced from ref [66] with consent from the Wiley, copyright 2022). C) The suggested reaction pathways, methane (CH_4), isopropanol ($(CH_3)_2CHOH$), ethanol (CH_3CH_2OH), and methanol (CH_3OH), are produced as a result of the electrochemical reduction of CO_2.

(Reproduced from ref [67] with consent from the Elsevier, copyright 2020). D) The proposed CO_2 electro-reduction process using the GO-VB_6-Cu catalyst is shown schematically. E-F) Faradaic Efficiency of CO_2 electro-reduction over several GO-VB_6-Cu catalysts at varying potentials. (Reproduced from ref [68] with consent from the Elsevier, copyright 2019). G) The appropriate energy barriers for the CuO_4 active region (red line) & Cu (111) actively site (blue line) to reduce CO_2 to *CO and *CHO intermediates. H) The equivalent energy barriers for pristine Cu (111) planes of lattice on Cu (111) @Cu-THQ to reduce CO to C_2H_4. (Reproduced from ref [69] with consent from the Royal Society of Chemistry, copyright 2021).

Cu@Cu_xO, a core@shell structured MOF-derived Cu catalyst, is employed by Kaili Yao and co-workers to convert CO_2 to ethylene. The oxidation state and surface area of the catalyst plays a significant role in the selectivity and enhance the electro-reduction of CO_2. The Cu^{2+} catalyst is reduced to Cu^+ and later Cu^0. The stabilized Cu^+ in the Cu^+/Cu^0 interfaces promotes *COCO dimerization, increases the selectivity of C_2 products, and suppresses the formation of C_1 products was shown in the **(Fig.12)**. The large surface of the metal-organic framework with a vast catalytic site enhances the CO_2 reduction reaction rate efficiency. With the incorporation of MOF and Cu active site properties, Cu@Cu_xO has exhibited 51% FE for the formation of ethylene and 70% FE for the formation of other C_{2+} products. Here, flow-cell configuration with a GDE increases productivity as in the convectional H-cell configuration; the mass transfer and current density is restricted by the low solubility of the CO_2 and the carbonate electrolyte.[71] Cu nanowires with high-density grain boundaries derived from Cu_3N for electro-reduction of CO_2 to C_2 products are reported by Yuying Mi and co-workers, with the high-density grain boundaries in the catalyst are essential for the active surfaces responsible for enhanced CO_2 reduction. The grain boundaries are formed due to the structural rearrangements caused by N^{3-} released during the reduction of Cu^{1+} to Cu. The Cu nanowire derived from Cu_3N demonstrates an outmost current density of -50.6 mA cm^{-2} at 1.0 V, which is higher than the Cu_3N nanowire. The 1D structure benefits the catalytic kinetics by providing a straight path for electron transfer, resulting in enhanced catalytic activity. An increase in FE is observed when the potential applied is increased from -0.5 to -1.0 V. The FE of 4% and 86% is observed for C_1 and C_2 products on the Cu nanowire catalyst. The Cu nanowire catalyst exhibited superior activity with high selectivity of C_2 products with FE of 8%, 12%, and 66% for C_2H_5OH, C_2H_6, and C_2H_4. It is concluded that the high selectivity of C_2 products is due to the availability of high-density grain boundaries was shown in the **(Fig.12)**.[51] Saranya Juntrapirom and co-workers have employed CuZn, a bimetallic electrocatalyst derived from carbonizing a MOF for conversion of CO_2 to C_2 products. The selectivity to form C_2 products is enhanced by blending Cu and Zn at varying ratios. The faradaic efficiency of CuZn nanoparticles has been increased 5-fold compared to the pristine Cu. Here, a polycarbonate H-type compression cell has been used

to perform electrocatalytic reaction. The catalyst's electrochemical active surface area and conductivity are increased by the presence of graphitic carbon formed during carbonization. Also, a decrease in surface area is observed in the carbonized samples, contributing to the diffusion of reactants to the reaction sites. The pristine Cu-C catalyst produces C_1 products like formate and CO, as Cu (111) shows high selectivity towards formate. When the concentration of Zn increases, the selectivity towards C_2 products increases. CuZn-C alloy exhibits a lower selectivity of formate at 6.9% FE and higher selectivity of C_2 products up to 14% FE at -1 $V_{RHE,}$ and the highest of 25% FE is observed, which is five folds that of Cu-C. The intimate surface contact between Cu and Zn facilitates the production of CO* intermediate, which favours the production of C_2 products than the C_1 product pathway was shown in the **(Fig.12)**.[72]

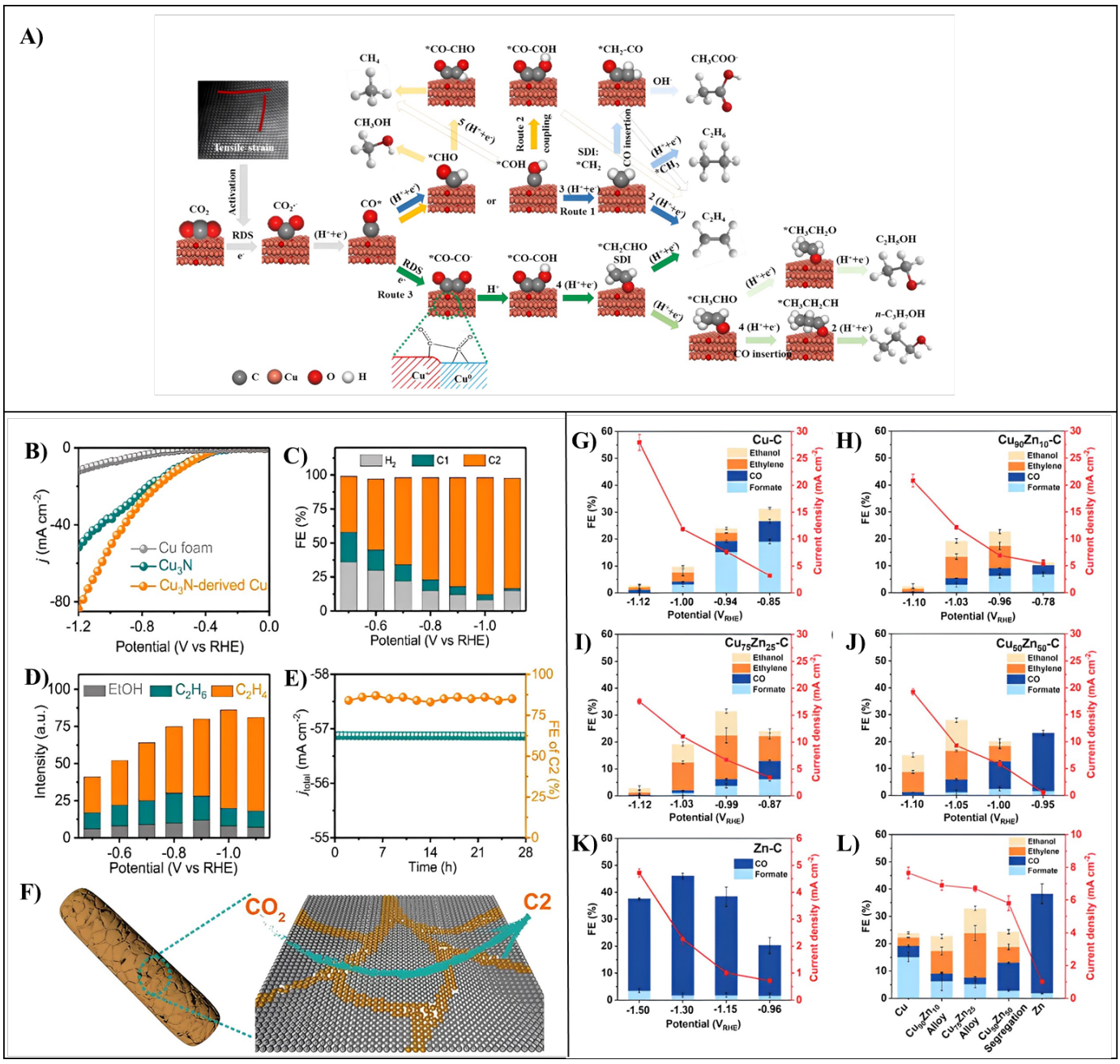

Fig.12 A) Proposed reaction pathways beginning at *CO on the Cu surface with Cu^{+}. Yellow, blue, and green paths represent rival replies. (Reproduced from ref [71] with consent from the Royal Society of Chemistry, copyright 2020). Characterization of the CO_2 electro-reduction process includes B) the measurement of LSV curves in CO_2-saturated solution C) the Faradic efficiency of H_2, C_1, and C_2 byproducts at various D) Faradic efficiency of EtOH, C_2H_4 & C_2H_6 products at applied potentials E) Chronoamperometry measurements at -1.0 V and various potentials F) Schematic depiction of the faradic efficiency of C_2 compounds on the Cu_3N-derived electrode, CO_2 electro reduction into C_2 products copper catalyst. (Reproduced from ref [51] with consent from the Wiley, copyright 2022). Various byproducts via catalyst G) Cu-C, H) $Cu_{90}Zn_{90}$-C, I) $Cu_{75}Zn_{25}$-C, J) $Cu_{50}Zn_{50}$-C, K) Zn-C and L) Cu_xZn_{100-x}-C at 1 VRHE**.** (Reproduced from [72] with consent from the Royal Society of Chemistry, copyright 2021)

CO_2 was electrochemically reduced to C_2H_4 on a copper hydroxide nitrate electrode reported by Mang Wang and co-workers with the molten salt decomposition method fabricated the electrode $Cu@Cu_2(OH)_3NO_3$. XPS and XRD data show that $Cu_2(OH)_3NO_3$ reduced to metallic Cu during the electroreduction of CO_2 in the $KHCO_3$ solution. This process leaves defects on the surface, favouring the selectivity towards C_2H_4. The high pH on the surface of the electrode suppresses the protonation of CO, resulting in less selectivity towards the formation of methane; FE < 2% is observed, which results in the high selectivity in the production of C_2H_4 with a FE of 31.80%. Also, an FE of 18.20% for formate is observed. The stability of the electrode is evaluated over 20h. FE of 30% for C_2H_4 is maintained, and a decrease in current density is observed during the stability cycle. The formation of C_2H_4 is deduced to occur in 3 different pathways. Initially, the *COOH intermediate is formed by electron and proton transfer which is further hydrogenated to give *CO. The path I propose is a C-C coupling between *CO intermediates. Path II proposes hydrogenation of *CO followed by C-C coupling between *CHO/*COH and *CO. Path III suggests dimerization of *CHO/*COH was shown in the **(Fig.13)**. This work opens a new area of study in the electroreduction of CO_2.[73] Chung Shou Chen and co-workers have proposed using Cu_2O-derived Cu and $PdCl_2$ sites for electroreduction of CO_2 to C_2H_6 by hydrogenation of $*C_2H_4$. The electropolished Cu electrode at negative potentials, FE of 40.1% for CH_4, is observed as the electron and proton transfer dominates. For Cu_2O derived Cu electrode, FE of 32.1% and 16.4% is observed for C_2H_4 and C_2H_5OH, respectively. CH_4 production is suppressed with FE of 1% at all potentials. The rise in local pH and morphological factors attributes to the selectivity towards C_2H_4. Also, FE < 1% is observed for C_2H_6. To boost the production of C_2H_6, $PdCl_2$ is added. Here, FE of 30.1% at -1.0 V is observed for the production of C_2H_6, and production of C_2H_4 is suppressed to FE 3.4%. The formation of C_2H_6 is elucidated as follows: On the Cu sites, CO_2 is reduced to C_2H_4. Through the $PdCl_2$ medium, C_2H_4 is hydrogenated to C_2H_6. The presence of $PdCl_2$ enhances the hydrogenation; it favors the adsorption of C_2H_4 on its sites. This study

proposes a new pathway for forming C_2H_6 from CO_2 rather than the conventional dimerization of CH_3 was shown in the **(Fig.13)**. [74] Oxide-derived copper has been employed by Louisa Rui Ling Ting and co-workersfor electroreduction of CO_2 to 1-Butanol. CuO-derived Cu GDE is used in a flow cell for alkaline electrolysis of CO_2 to form C_4 products. 1-butanol is formed by two-step electro-reduction of crotonaldehyde, formed by aldol condensation of two acetaldehyde molecules generated from the conversion of CO_2. FE of 0.056%, the current density of -0.080 mA cm^{-2} at -0.48 V is observed for forming 1-butanol in contrast to the conventional mechanism of C-C coupling, where acetaldehyde plays a significant role was shown in the **(Fig.13)**. In this work, alkaline catalyzed aldol condensation, crotonaldehyde plays a prominent role which is electrochemically reduced to 1-butanol.[75] Jinmo Kim and co-workers have developed CuO nanoparticles for electroreduction of CO_2 to ethylene. Here, two different morphologies of CuO nanoparticles, i.e., branched and cubic, have been employed to examine the effect of morphology on the selectivity of the reduction product. In 0.1 M $KHCO_3$, at low potentials, FE of 50% at -0.7 V is obtained for CO using branched CuO. At high potentials, the production of CO is suppressed to FE 5%. Selectivity towards the formation of ethylene increased to FE 53%. In contrast, the cubic Cu_2O catalyst produces CO and ethylene in similar trends with low FE. The evolution of H_2 is significant at all potentials, with an FE of 42%. When the electrolyte concentration is increased to 0.5 M $KHCO_3$, the selectivity towards ethylene decreases to FE 36%. On the other hand, the evolution of H_2 is increased to FE 53%. In the presence of cubic Cu_2O, FE of 24 and 75% is observed for the formation of ethylene and H_2, respectively was shown in the **(Fig.13)**. At a long-time reaction with branched CuO, the FE of ethylene is increased to 70% at 550 min. After 720 min, the FE of ethylene is decreased and maintained at 65%. In cubic Cu_2O, the FE of ethylene is decreased to a negligible value at 10 h. The branched CuO has a large surface area with a highly active surface. Thus, it shows superior activity than cubic Cu_2O. This study paved the way for the commercial application of electroreduction of CO_2. [76] Andrews Nirmala Grace and co-workers have reported polyaniline/Cu_2O composite for electro-reduction of CO_2 to formic acid and acetic acid. Throughout 2hrs in Tetrabutylammonium (TBAP) electrolyte at -0.3 VFE of 63 and 30.4% is observed for the formation of acetic acid and formic acid, respectively. After the reaction, the FE declined to 19.2% and 7.7% for formic acid, respectively. The formed product has been confirmed by performing analytical techniques, including GC-MS, Proton Nuclear Magnetic Resonance (H NMR), HPLC, and Ion Chromatography (IC).

$$H^+ + e^- \rightarrow H_{ad}CO_2 + H_{ad} \rightarrow HCOO_{ad}HCOO_{ad} + H_{ad} \rightarrow HCOOH \quad (15)$$

$$HCOO_{ad} + CH_3OH \rightarrow CH_3COOH + OH_{ad} \quad (16)$$

$$OH_{ad} + H_{ad} \rightarrow H_2O \quad (17)$$

Here, the solvent methanol attacks the formic acid to produce acetic acid. This study demonstrates a new method to produce formic acid from inexpensive raw materials.[77]

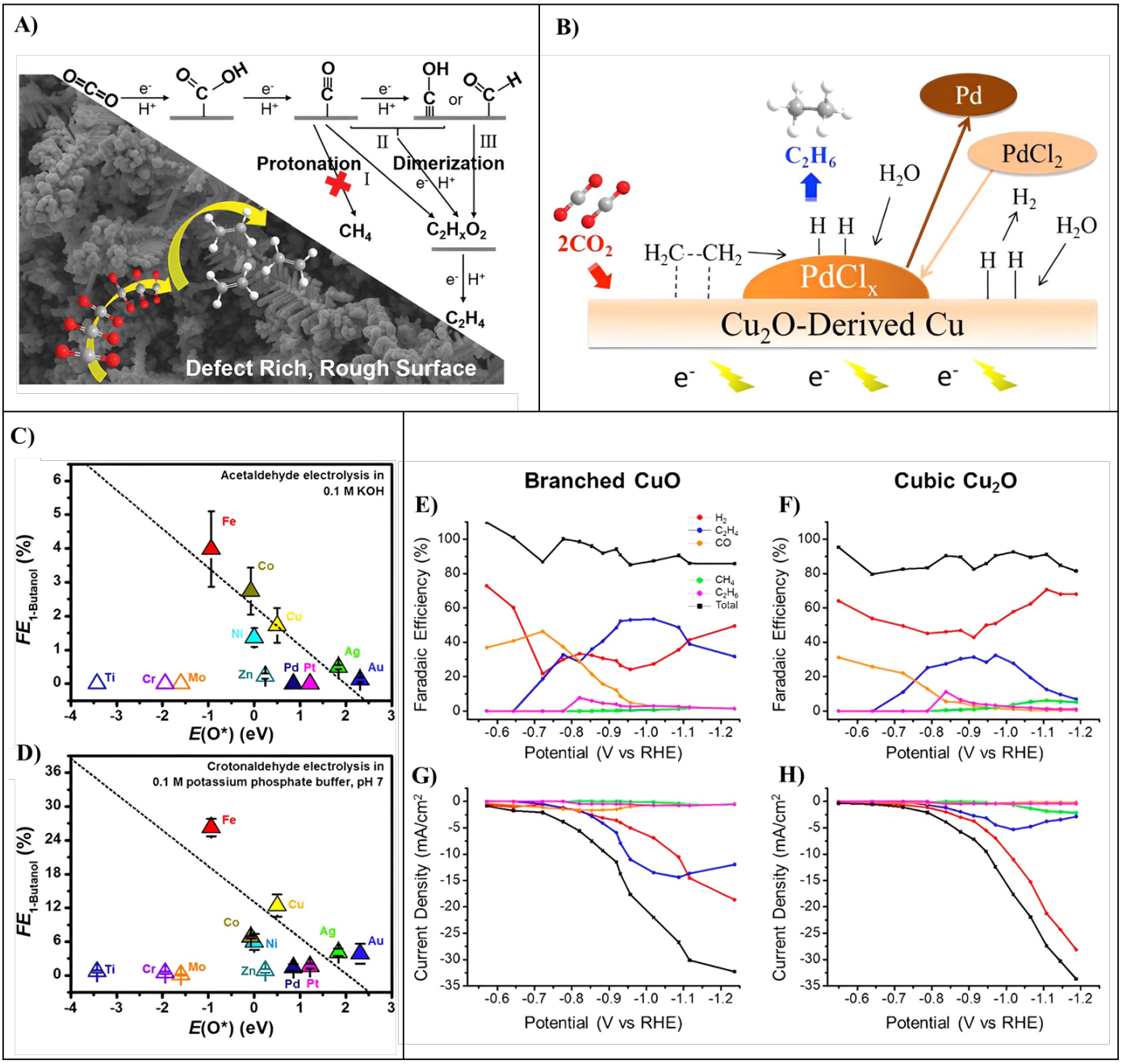

Fig.13 A) The electroreduction of CO_2 to ethylene on the Re-Cu@$Cu_2(OH)_3NO_3$ electrode is shown in the diagram. (Reproduced from ref [73] with consent from the Royal Society of Chemistry, copyright 2020). B) Diagram showing how CO_2 is reduced electrochemically to C_2H_6 through an adsorption C_2H_4 intermediate. (Reproduced from ref [74] with consent from the American Chemical Society, copyright 2015). Based on the DFT-calculated adsorbed oxygen stability on these metals concerning the faradaic efficiencies of 1-butanol from -10 mA cm^{-2} constant-current electrolysis of C) acetaldehyde and D) crotonaldehyde on specified metals about hydrogen and water usually, oxides metals at 0 V against. RHE Hollow symbols that

represent the pH of the supporting electrolyte are displayed. 1-Butanol was not found when electrolyzing acetaldehyde on titanium, copper, gold, and platinum. (Reproduced from ref [75] with consent from the Wiley, copyright 2020). Copper oxide nanoparticle electrocatalytic profiles using (E, G) branching CuO and (F, H) cubic Cu_2O nanoparticles. the plot in (E, F) and (G, H) show FEs and current densities for H_2, ethylene, CO, and methane at various applied potentials. (Reproduced from ref [76] with consent from the American Chemical Society, copyright 2019).

Cu nano dendrites have been employed by Minfang Wu and co-workers for electro-reduction of CO_2 to C_2 and C_3 products. Initially, Copper phosphate flakes were synthesized, and Cu^{2+} in the flakes was reduced to Cu^0 by applying negative potentials. At this stage, a change in color from blue to brown carbon paper is observed. This leads to the formation of nano dendrites. The electroreduction of CO_2 gives products C_1 products, including CO, methane, and formic acid, C_2 products, including ethylene and ethanol, and C_3 products, including propanol and propanal. Also, competitive H_2 production is observed. At -0.8 V, H_2 production FE of 62.4 and 34.4% is obtained over Cu particles and Cu NDs, respectively. At lower potentials, the FE of H_2 remained at ~23% for Cu NDs and ~44% for Cu particles. This concludes that the competitive HER is suppressed by employing Cu NDs. Among the formation of C_1 products, the FE of formate production is similar among Cu particles and Cu NDs. At -0.8 V, the FE of CO over Cu NDs is 4.5 times higher than that of Cu particles. In contrast, the FE of CH_4 over Cu particles is 35% higher than that of Cu NDs. This states that Cu NDs are highly selective for forming CO, which is the building block for forming C_2 products. At -1.2 V, FE of 22.3% and 13.0% is obtained for forming C_2H_4 over Cu NDs and Cu particles, respectively. FE for forming n-PrOH and propanal over Cu NDs are 3.1% and 2.9, respectively was shown in the **(Fig.14)**. By applying more negative potential, it is observed that the Cu NDs are more favourable for forming C_2 products with higher FE than Cu particles. Cu NDs favor the dimerization of CO intermediates to give C_2H_4. Further insertion of CO leads to the formation of C_3 products. This study gives insights into the feasible approach to forming valuable multi-carbon products via the electroreduction of CO_2. [78] Xiaona Ren and co-workers have reported Cu_v-Cu_2O catalyst with abundant Cu vacancies for electro-conversion of CO_2 to C_2 products. Cu vacancies on Cu_2O surface modifies the electronic structure and interact with the significant intermediates, enhancing the conversion of CO_2 and selectivity towards forming C_2H_4. High selectivity towards C_2H_4 is achieved by the strong adsorption of *COH and weak affinities of *Co and $*CH_2$ by the Cu vacancies on the Cu_2O surface was shown in the **(Fig.14)**. Maximum selectivity of C_2H_4 is obtained with FE of 51.0% and is achieved at -0.76 V as the potentials become more negative. Also, the adsorption of key intermediates like *COH, *CO, and $*CH_2$ by Cu vacancy on Cu_2O surface limits the required reaction energy, so selectivity towards C_2H_4 increases and inhibits the side

reactions. This works as a hopeful strategy to increase the activity of CO_2 reduction towards C_2 product selectivity by vacancy engineering.[79]

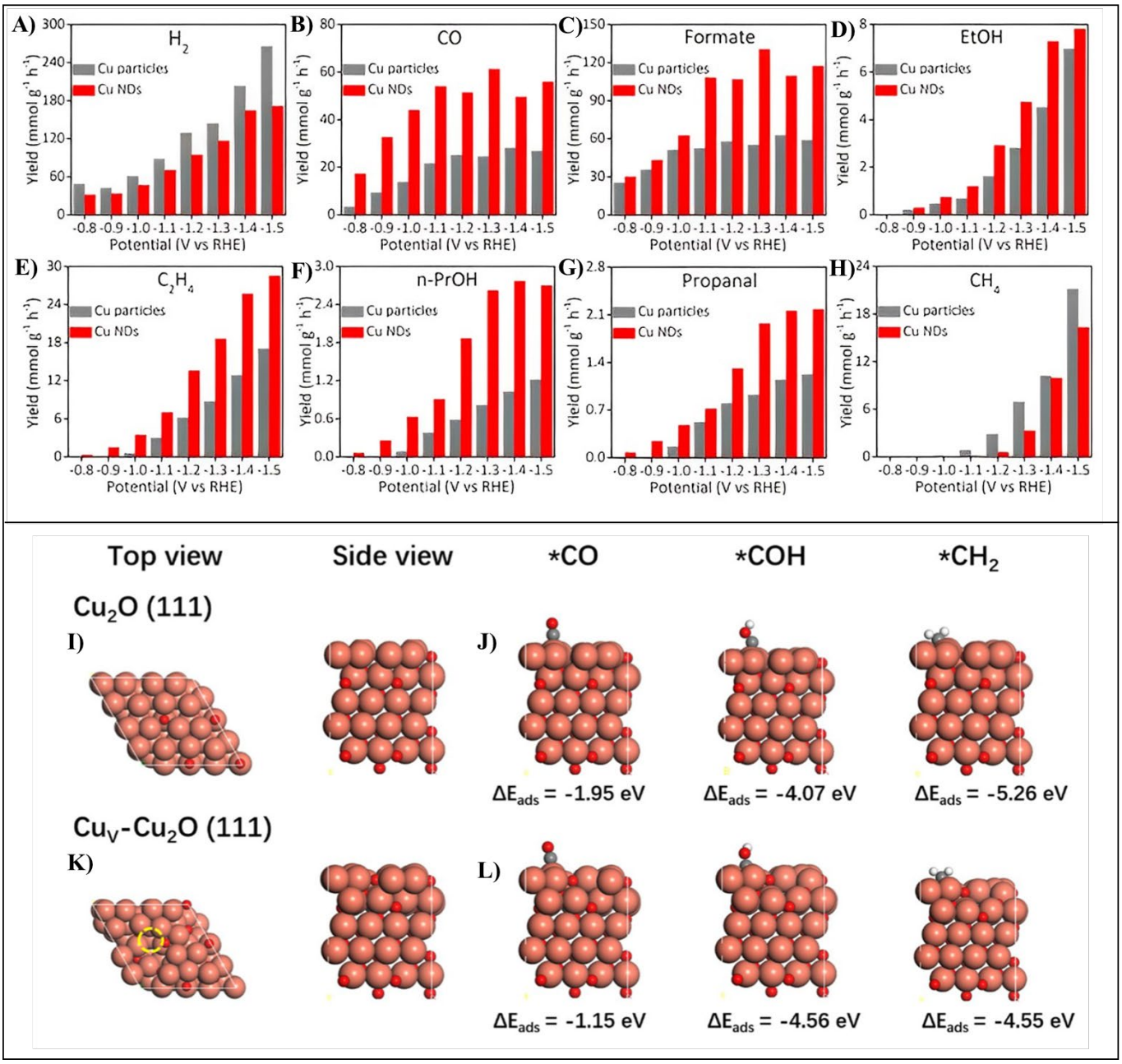

Fig.14 Yields of the Obtained products over the Cu particles and the Cu NDs: A) H_2, B) CO, C) formate, D) EtOH, E) C_2H_4, F) n-PrOH, G) propanal, and H) CH_4**.** (Reproduced from ref [78] with consent from the American Chemical Society, copyright 2020). The adsorption energies of the three important intermediates *CO, *COH, and *CH_2 on the surfaces of the catalysts I-J) Cu_2O (111) and K-L) Cuv-Cu_2O (111). (Reproduced from ref [79] with consent from the Elsevier, copyright 2020).

Cu catalyst derived from Cu_2O is employed for electroreduction of CO_2 by Yun Huang and co-workers Here, reduction activity is compared with Cu_2O derived Cu catalyst and Cu single crystal surface. At Cu_2O derived Cu electrode, FE of 32.4% at -0.98 V is observed for forming C_2H_4, and FE < 2 % at -1.13 V is observed for forming CH_4. These results show a remarkable selectivity towards C_2H_4. At Cu (100), on lower over potential H_2 production is dominant with a FE of 67-94%. With increased overpotential, the production of H_2 is suppressed, and selectivity towards C_2H_4 increases. FE of 30.6% is observed for C_2H_4 at -1.30 mA/cm^2. Here, selectivity towards CH_4 with a FE of 43.5% at -1.15 V. Cu (110) shows excellent selectivity towards formate with FE of 24.7% at -0.8 V. Cu (100) achieved formation for C_2H_4 as it has high coverage of *CO and forms dimerization pathway to produce C_2H_4 was shown in the **(Fig.15)**. This work gives insights into the role of the Cu surface in conciliating the C_1 intermediate to C_2H_4. [80] Dan Ren and co-workers have developed Cu_2O as an electrocatalyst for converting CO_2 to C_2 products. By galvanostatic deposition method, Cu_2O films are formed at different thicknesses. Scanning Electron Microscopy (SEM) micrographs estimate the thickness of the film. The CO_2 reduction reaction is carried out at a potential ranging from -0.59 V to -1.19 V. Electropolished Cu electrode at -1.19 V, FE of 59% is observed for CH_4. On thicker films, the production of CH_4 is drastically decreased to FE < 2%. At -0.99 V, the Cu_2O catalyst showed high selectivity toward forming C_2 products. FE of 22-40% and 4-16% are observed for ethylene and ethanol, respectively. The Cu_2O film with a 1.7-3.6 μm thickness, selectivity towards C_2 products is optimum with FE of 34-39% and 9-16% for ethylene and ethanol respectively. The FE of ethylene is always higher than that of ethanol. This indicates that the two products formed from a common reaction intermediate. From the DFT calculation, it can be proposed that $*CH_2CHO$ is the key intermediate was shown in the **(Fig.15)**. The increased local pH on the electrode's surface also contributes to the selectivity towards forming C_2 products. The local pH is not the sole factor contributing to the selectivity, and the morphological factor also dictates the selectivity. It is observed that the FE of C_2H_4 is decreased with increasing thickness of the film at 6.4 and 8.8 μm. This work demonstrates the selectivity factor in the production of C_2 products. [81] Cu_2O-derived Cu catalyst has been employed by Albertus D Handoko and co-workers for the electro-reduction of CO_2 to C_2H_4. FE of 31, 16, and 1-2% is observed for forming C_2H_4, C_2H_5OH, and CH_4, respectively. At lower overpotential, the selectivity towards C_2H_4 is higher. For instance, FE of 15 and 31% is observed for forming C_2H_4 at overpotentials of -0.83 and -0.98 V, respectively. Here, two major factors contribute to the selectivity of C_2H_4: local pH and morphological factors. It is observed that the local pH is directly proportional to the selectivity of C_2H_4, and the crystalline size is inversely proportional to the selectivity toward the formation of C_2H_4. The formation of ethylene is described as, at first, CO or CHO being formed from the reduction of CO_2. The C-C coupling of these formed intermediates gives C_2 adsorbates, and further hydrogenation leads to the formation of C_2H_4. The yield of the reduction products of CO_2 can be optimized by altering the applied current density. At ambient

pressure, it is observed that for total CO_2 reduction, the FE can be optimized to 70.1%, where FE of 42.6, 11.8, and 5.4% correspond to the reduction products, such as ethylene, ethanol, and n-propanol. This work pinpointed the relationship between the morphological factor and selectivity toward forming C_2 products was shown in the **(Fig.15)**. Also, this study opened a new avenue for optimizing the yield of reduction products. [82]

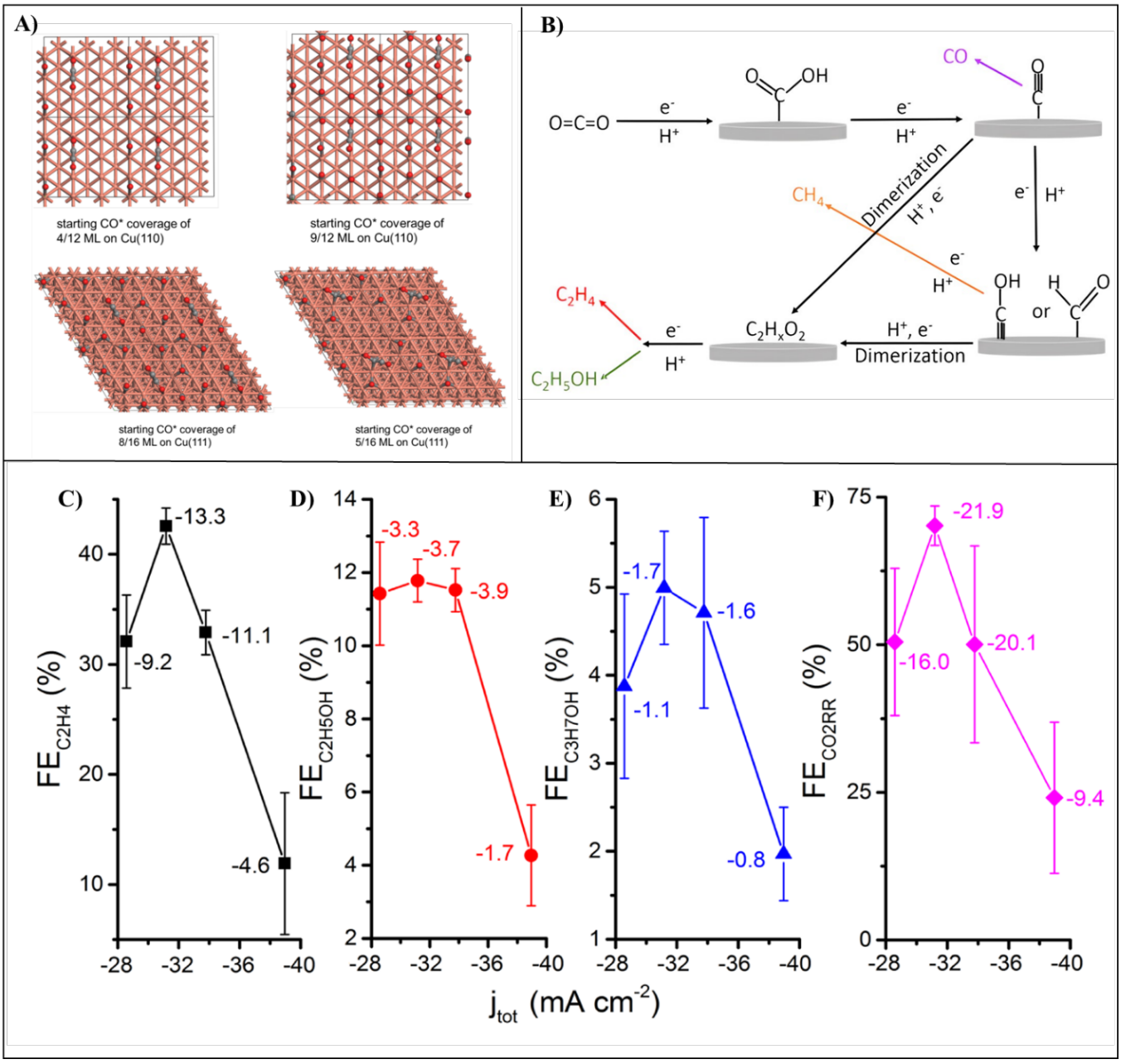

Fig.15 A) Adsorption structures of OCCO* (top view) on surfaces of Cu (100), Cu (110), and Cu (111). (Reproduced from ref [80] with consent from the American Chemical Society, copyright 2017). B) Ethylene and ethanol electroreduction of CO_2 to be carried out on copper surfaces. Hydrogen atoms are not drawn. (Reproduced from ref [81] with consent from the American Chemical Society, copyright 2015). The maximum limited charge density of C) ethylene, D) ethanol, E) n-propanol & F) total CO_2 reduction

products can be measured using chronopotentiometry on Sample C at a limited jtot range of between -28.6 and -39 mA cm^{-2}. The limited current density of the associated product, expressed as mA cm^{-2}, is shown by the numbers mentioned adjacent to the data points. (Reproduced from ref [81] with consent from the American Chemical Society, copyright 2016).

Martina Serafini and co-workers have reported that the nanostructured materials CuMgAl Layered Double Hydroxide (LDH)-based material using a 4 cm^2 carbon-based gas diffusion membrane. A composite boasting close interaction between a ternary CuMgAl LDH and Cu^0 /Cu_2O species may be obtained via a one-step, repeatable potentiodynamic deposition. In addition, the molar proportion of the total quantity of bivalent cations and Al^{3+} in the electrolyte, the volume being loaded, and the molar proportions of the three cations (CuMgAl 2:1:1 LDH-CP) in the electrolyte. The fundamental issue with C_1 products remained their low selectivity, although CuMgAl LDHs based materials perform better in C_1 selective products. The electrocatalyst was evaluated in the liquid phase of CO_2ER during a 1h reaction at -0.4 V vs RHE, specifically to assess the selectivity towards acetic acid generation. The Cu_0/Cu_2O particles are presumably more coated by non-redox reactive elements (Mg and Al), causing a shift at the interface of the electrode and electrolyte that negatively impacts the catalytic activation reactions. With the lowest crystallite sizes and the greatest crystalline structure, the electrocatalyst produced the highest amount of CH_3COOH. Specifically, the output from 1.1 mmol CH_3COOH $gcat^{-1}$ h^{-1} produced by the CuMgAl 1:2:1 LDH/CP catalyst to 2.0 mmol CH_3COOH $gcat^{-1}$ h^{-1} produced by the CuMgAl 2:1:1 LDH/CP catalyst was shown in the **(Fig.16)**. The potential benefits of mixing Cu^0/Cu^+ species with an alkaline material like LDHs, which has a high affinity for CO_2, since this combination increases the availability of carbon sources at the electrode and functions as a redox mediator by converting CO_2 into C_2 product.[83]

Recently, it was demonstrated by introducing a copper-based catalyst generated from phosphate (PD-CuO_x/C) for effective CO_2ERR towards C_{2+} production synthesized by in situ rebuilding from Tengfei Gao and co-workers. Reconstruction techniques are used to PD-CuO_x/C samples, demonstrating the creation of copper phosphate in addition to the matching, widely spaced Copper nanoparticles produced via electroreduction. Cu nanoparticles that are well-dispersed in PD-CuO_x/C facilitate the C−C couplings of essential CO_2ERR intermediates, hence promoting the formation of C_{2+}. The performance of PD-CuO_x/C in CO_2ERR a noticeable increase in C_{2+} productions and a noticeable decrease in the amount of HER for as low as about 30% FE (H_2), which suggests that the PD-CuO_x/C samples had more favourable CO_2ERR activities. The FEs of formate and CO for C_1 products reached an ultimate value of around 55% between −0.8 and −1.0 V. Still, the FE for C_{2+} products continued to rise with progressively raised potentials, indicating that PD-CuO_x/C has a preferred C−C coupling capacity. Over PD-CuO_x/C, an ultimate FE (C_{2+}) of 45% has been achieved at −1.4 V. Through PBS treatments during in situ reconstruction, the C_2H_4 yield

was enhanced approximately 20 times, rising from 1.9 × 103 μmol h^{-1} cm^{-2} into CuO/C to 2.6 × 104 μmol h^{-1} cm^{-2} over PD-CuO/C. Additionally, the ethanol yield improved roughly 10 times, rising from 0.7 × 103 μmol h^{-1} cm^{-2} over CuO/C to 8.8 × 103 μmol h^{-1} cm^{-2} over PD-CuO/C was shown in the **(Fig.16)**. The PD-CuOx/C C_{2+} production performance is similar to that of the H cell-generated Cu catalysts. In addition to the Cu^{+} species that are stabilized in PD-CuO_x/C, the phosphate-derived Cu essence is also responsible for the enhanced CO_2ERR performance in the formation of C_{2+} products.[84] Apurv Saxena and co-workers have reported that an effective electrocatalytic CO_2 reduction catalyst has been determined to be copper cobalt selenide ($CuCo_2Se_4$). It shows good selectivity for products with high carbon content and added value. Compared to binary selenides, it was shown that the catalyst's activity towards CO_2RR was increased by the concurrent presence of Cu & Co. Moreover, $CuCo_2Se_4$ showed a high degree of product selectivity, only generating carbon-rich products at low applied voltage, including ethanol and acetic acid. Compared to binary Cu or selenides, the CO energy from adsorption was in the ideal range. Additionally, it demonstrated that Cu possesses superior adsorption and selectivity for intermediate CO as compared to Co. The $CuCo_2Se_4$ matrix's superior electrical conductivity and the easy adsorption to intermediary CO on the catalyst surface may result in increased product selectivity at low applied potentials. For different applied potentials between (-0.1 and -0.9 V) vs RHE. More significantly, it was shown that at lower applied potential (−0.1V), the $CuCo_2Se_4$ modified electrode could yield unique C_2 products such as acetic acid & ethanol having 100% faradaic efficiency shown in the **(Fig.16)**. C_1 products like methanol and formic acid were formed at larger applied potentials (−0.9 V), whilst C_1 products were obtained up to (−0.3 V). This catalyst's great selectivity and predilection for the production of acetic acid & ethanol draw attention to its uniqueness. As a result, the very effective CO_2 reduction catalytic activity of $CuCo_2Se_4$ also provides a proper understanding of the surface of the catalyst design and how to achieve such high selectivity.[85] Lin-jun Zhu and co-workers have reported that effective C-C coupling with Cu nanoparticle catalysts necessitates the cooperative activation of adsorbed C_1 products on two metal sites. To create C_{2+} selective molecules ECR catalysts, it is preferable to build paired or dimer sites with intentional ligand frameworks. The Cu (I)/Cu (II) redox pair is responsible for the quasi-reversible peaks that the Cu-(salophen)-coated electrode displays at 0.44 V (cathodic) and 0.83 V (anodic) vs RHE in an N_2 environment. Several products were identified, including n-propanol, acetate, ethanol, formate, carbon monoxide, methane, and ethylene. With hydrogen's faradic efficiencies (FEs) being below 40%, there was a partial suppression of hydrogen evolution in the potential range of -0.5 to -1.2 V vs RHE. Two-electron reduction products, namely formate and CO, are the main products in the low overpotential area. Over 50% of CO faradic efficiencies occur between -0.5 and -0.7 V vs RHE. Similar to C_2H_4, other C_{2+} products including ethanol, n-propanol, and acetate exhibit partial current densities and FE patterns. With a partial current density of 121 mA/cm^2, the total FE for all C_{2+} products like ethylene, ethanol, n-propanol, and acetate were maximized at −1.1 V vs

RHE. All C_{2+} products had a minor reduction in total FE to 37% at −1.2V vs RHE, but an increase in partial current density to 124 mA/cm^2. As a result, one of the rare meric ECR electrocatalysts that prefers C_{2+} products are the Cu− superamolecular pair catalyst. Cu-based materials exhibit a crucial stage in the emergence of the C_{2+} product, known as CC coupling, which may be enhanced by building metal–metal-supramolecular couples (π-π) via stacking was shown in the **(Fig.16)**.[86]

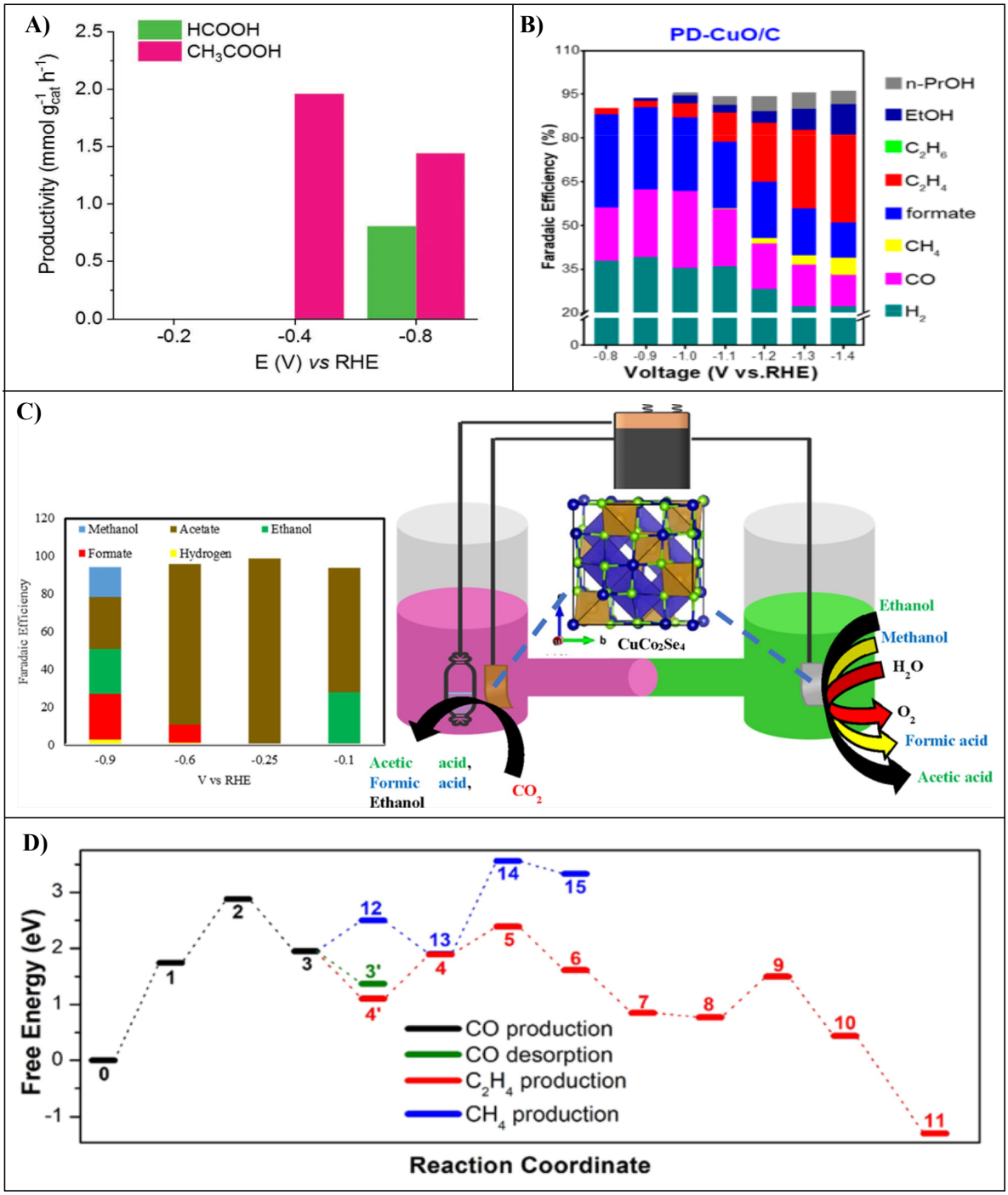

Fig.16 A) CO_2ERR product distribution utilizing the CuMgAl 2:1:1 LDH/CP during a 1h reaction at various applied potentials. (Reproduced from ref[83] with consent from Wiley, copyright 2023). B) The

CO_2ERR outcomes pertain to the PD-CuO_x/C samples. (Reproduced from ref[84] with consent from the American Chemical Society, copyright 2023). C) Plots showing the relative amounts of liquid products at various stationary applied potentials that were measured using NMR. (Reproduced from ref[85] with consent from the American Chemical Society, copyright 2023). D) Energy identities for CO_2 reduction catalyzed by Cu(salophen) to produce CO, CH_4 & C_2H_4. (Reproduced from ref[86] with consent from the American Chemical Society, copyright 2023).

Na Liu and co-workers have reported that a short Cu-Cu distance heterogenized binuclear hydroxo-bridged phenanthroline Cu (II) molecule has been described as an easy-to-use but effective catalyst for the electro generation is ethylene and other C_2 products. The catalyst shows a favourable shift in the reductive current's start and a greater current concentration of −5.5 mA cm^{-2} at −1.2 V vs RHE in the CO_2-saturated electrolyte, suggesting that CO_2RR has a promising catalytic activity. In a CO_2-saturated solution, regulated potential electrolysis was carried out for 30 minutes at possibilities between −1.35 & −1.10 V vs RHE. With the greatest FE at −1.25 V, C_2H_4 is generated with relatively little variance (33–42% FE) over the whole potential domain. Assuming two hydroxo-bridged Cu centers as the active site, the average charge density at −1.25 V is 6.3 mA cm^{-2}, which translates into an average of 10.5 h^{-1} about ethylene production. On the other hand, CO production is only noticeable at lower negative potentials and stops in favor of CH_4 as the driving force increases. Notably, Catalyst prefers CO_2RR over HER, as evidenced by the selectivity for H_2 being ~10% or lower over the whole potential domain. the product selectivity of H_2, C_1, and C_2 at various potentials. The overall FE for C_2 products, which include C_2H_4 (FE = 42%), C_2H_5OH (FE = 12%), CH_3CHO (FE = 6%), and CH_3COOH (FE = 2%), reaches 62% at −1.25 V vs RHE was shown in the **(Fig.17)**. The FE for C_1 goods is as low as 30% at the same potential. After 15h of continuous electrolysis, the binuclear hydroxo-bridged phenanthroline Cu (II) molecule shows excellent stability with no discernible degradation.[87] Anna Loiudice and co-workers have reported the impact of Cu nanocrystal's (NCs) size and shape on both their CO_2 electroreduction efficiency and product selectivity. Cu NC spheres in two distinct diameters. Three distinct sizes of Cu NC cubes (24 nm, 44 nm & 63 nm) and (7.5 nm and 27 nm) were created using the same colloidal chemistry-based technique. There was a tendency towards non-monotonic selectivity, with 80% selectivity towards carbon products and 50% of them being ethylene. The activity for HER and CO_2RR is equivalent in the smaller cubes ($FECO_2RR$ = 50%), with the main carbonaceous species being formate and methane (C_2H_4-CH_4 = 0.63). Each of the three metrics of merit gets better as the cubes get bigger. With the highest selectivity towards CO_2RR ($FECO_2RR$ = 80%) and ethylene as the main reduction byproduct (FEC_2H_4 = 41%, C_2H_4-CH_4 = 2.03), the cubes with 44 nm edge length performed the best. While there was a minor rise in C_2H_4-CH_4 in the biggest cubes, there was a drop

in overall CO_2RR activity and a decrease in ethylene production (FEC_2H_4 = 25%). To further increase the selection regarding CO_2RR and towards C-C coupling, ultrathin architectures and nano frames with an abundance of edge atoms may be desired as shown in the **(Fig.17)**. This study is fundamental in establishing the adoption of atomically specified colloidal NCs as a nanomaterial platform for furthering CO_2 reduction, given the potential of colloid chemistry to access a broad compositional space.[88] Wei Zhang and co-workers have reported the C–C coupling that occurs in the electrocatalytic CO_2 reduction reaction (CO_2RR) is a characteristic feature of highly related OBC systems and might be advantageous for several other Cu-based catalytic processes, oxygen-bearing copper (OBC) is extensively researched for this purpose. At around −0.95 V, the OBC sample has the greatest C_2H_4 Faradaic efficiency, measuring approximately 45%. A flame ionization detector (FIDs) gasoline chromatography (GC) traces of gaseous products demonstrate the significant suppression of CO_2 reduction to methane or carbon monoxide at -0.95 V. This suggests that CO has dimerized over its potential of -0.65 V over OBC. On the other hand, CH_4 is the main CO_2RR product for the OFC sample used for control above the potential of -0.65 V. Among the three catalysts, the OBC sample consistently shows the highest C_2H_4 fractional current densities at all specific potentials. Remarkably, the onset potential of C_2H_4 at OBC has a value of approximately −0.54 V, which is higher than that of its oxygen-free copper micropore nanowires (OFC) equivalent, which is −1.01 V. Furthermore, the C_2H_4 partial charge density of 44.7 mA cm^{-2} at −1.00 V for the OBC sample is observed, which is about 26 and 116 times greater than that of the OFC and Cu foam samples, respectively was shown in the **(Fig.17)**. The HOMO peak of the OBC (Cu_4O) d states changes to the right somewhat following the CO_2 adsorption, based on the density of states data. When compared to O-loss OBC, the HOMO peak intensity of O-loss OBC increases noticeably with CO_2 adsorption. This suggests that the surface Cu atom's d-states associated with the vacancy can be enhanced by CO_2 adsorption, which might account for the vacancy's strong connection with the CO_2 molecule. The oxygen-bearing copper surface, which promotes CO adsorption as well as dimerization and therefore intensifies the C–C coupling process, is the source of the enhanced C_2H_4 selectivity. This work should be helpful for a wide range of additional Cu-based catalytic processes, many of which are thought to happen on partially oxidised Cu surfaces. These processes include methane activation, water-gas shift, catalytic oxidation of substances (CO, alcohols, olefins, etc.), and catalytic oxidising (CO, alcohols, etc.).[89] Roham Dorakhan and co-workers have reported that the catalyst design technique destabilizes on-target intermediates (including variables such as ethanol and ethylene) in the reduction of carbon monoxide to acetate. This off-target intermediate destabilization results in an acetate on the optimized Ag–CuO_2 catalyst. Combine the system architecture and catalyst to reduce the cost of liquid separation while simultaneously enhancing the reaction kinetics. There is a two-step method for acetic acid electrosynthesis that calculates that if an elevated energy efficiency (EE) is attained, the amount of greenhouse gas emissions produced will be reduced by around ten times. using low-carbon (wind, 6

gCO_2ekWh^{-1}) power and utilizing fuel that is CO_2 or CO generated from it. A kinetically limited galvanic replacement technique to create distinct active-site landscapes and alter the outermost Ag content in a succession of Ag–Cu_2O catalysts. At the ideal Ag: Cu loading, the Ag–Cu_2O catalysts achieved an acetate FE of 70% and a maximal partial current density of 310 mA cm^{-2}. Due to the presence of grain boundaries created through the in-situ reduction, oxide-derived Cu allows for C–C interaction. Acetate productivity rose in Ag–Cu_2O samples with increasing Ag content, but at the expense of ethylene, ethanol, and hydrogen. There was an accompanying rise in acetate from 10% to 15% along with a drop in ethylene & hydrogen FE from 40% to 35% and 15% to 13%, respectively. CuAg active areas with distinct selectivity favoring C_2 products than Cu are shown by this shift in C_2 selectivity upon increasing Ag loading was shown in the **(Fig.17)**. The system produced 5-weight percent acetate at 100 milliampere-seconds and a full-cell energy efficiency of 25%, which is a twofold improvement over the most energy-efficient electrosynthesis. Ag–CuO_2 catalyst, this destabilization of off-target intermediaries leads to an acetic acid Faradaic efficiency at 70% at 200 milliampere-seconds and 18 hours of reliable operation in a membrane-based electrode assembly.[90]

Yoshio Hori and co-workers developed the efficient generation of CH_4, C_2H_4, and alcohols during the electrochemical reduction of CO at copper electrodes amid aqueous inorganic salt solutions. In the effluent gas, the gaseous products CH_4, C_2H_4, CO, and H_2 were visible. The gaseous byproducts were not seen before the initiation of the electrolysis process. During the electrolysis, the quantities were almost constant; in an average experiment ($KHCO_3$, CH_4) -202 ppm, (C_2H_4) -139 ppm, and H_2 -(386 ppm) were all present at 0.1 mol dm^{-3}. There was no C_2H_6 found in the discharge gas. The electrolytes contained the products HCO_2^-, Pr^nOH, and EtOH. There was no CH_3OH found in the mixture. HCHO was not examined following the initial CO_2 stage of the investigation. In a control experiment with the same setup but no electrolysis, the soluble compounds were not detected within the permissible range of detection. The incorporation of CO into a surface carbene is a process involved in the creation of ethanol. The electroreduction for CO on a Cu electrode may use a similar procedure. The CH_2 (ads) combines with CO to first reduce to CH_2=C=O(ads), then to CH_2=CH-OH (ads), and finally to CH_3CH (ads). Ultimately, these intermediates are converted to n-C_3H_7OH and C_2H_5OH. The pH at the contact point controls the availability of protons or hydrogen on the surface, which affects product selectivity. Because OH-is produced during electrode reactions, the electrolyte has a significant impact on the electrode's pH. The Fischer-Tropsch reaction's mechanism and the synthesis of alcohols and hydrocarbons are compared.[91]

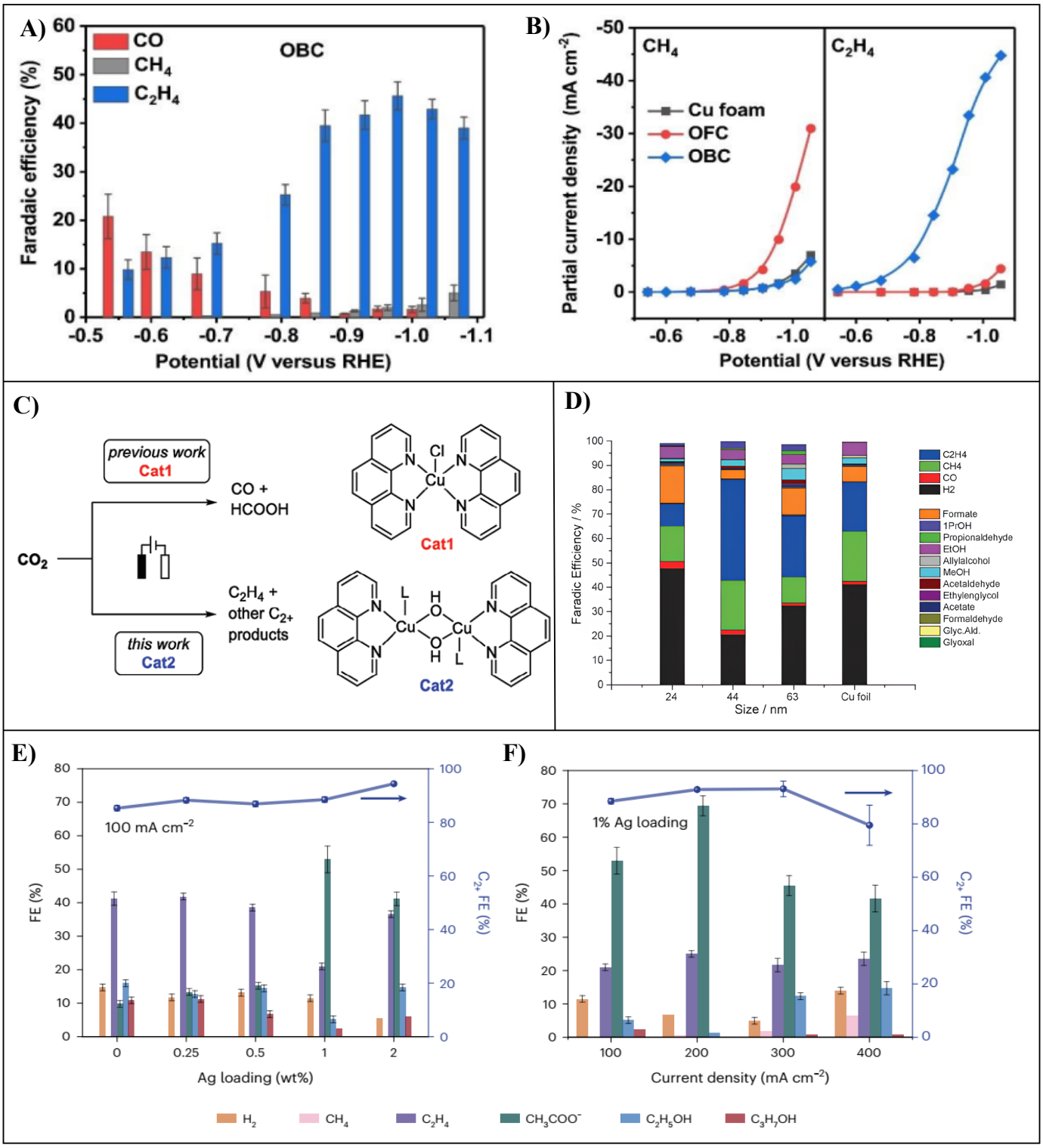

Fig.17 A) Main CO_2RR product's faradaic efficiency on OBC and OFC B) Partial current densities on Cu foam, OFC, and OBC towards CH_4 (left) & C_2H_4 (right). (Reproduced from ref[89] with consent from the American Chemical Society, copyright 2020). C) Cu phenanthroline compounds for CO_2RR that are mono- and binuclear. (Reproduced from ref[87] with consent from Wiley, copyright 2023). D) A bar chart showing the faradaic efficiency for each product in Cu foil at 1.1 V vs RHE and in various sizes of Cu NC cubes. The signal of glassy carbon has been removed. (Reproduced from ref[88] with consent from Wiley, copyright

2016). E) FEs for methane, hydrogen, ethylene, acetate, ethanol, and propanol on a three-electrode flow cell undergoing CO electroreduction at 100 mA cm^{-2}. F) The CORR products FE distribution for the Ag1%–Cu_2O electrocatalyst at various current densities. (Reproduced from ref[90] with consent from Nature, copyright 2023).

While the Kaisong Xiang and co-workers designed the catalyst with iodine doping on the copper catalysts to boost C_2H_6 production, wherein they constructed the Cu_xO-derived Copper catalyst nanoarrays are utilised to provide a controlled microenvironment that facilitates the supply of C_2H_4 for the generation of C_2H_6. In addition to greatly exposing the active sites and producing a high pH inside the nanoarrays, the nanoarrays will establish a microenvironment to speed up the flow of electrons and reactants, which in turn facilitates the C_2H_4 formation with C-C coupling. Subsequently, incorporate iodide into Cu nanoarrays obtained from CuxO, so facilitating the hydrogenation of the resulting C_2H_4 to C_2H_6 by the action of iodide. By employing an elaborate electrode design, we successfully enhanced both the C_2H_4 feeding capacity and C_2H_4 hydrogenation capability. As a result, we attained a Faradaic efficiency of 24% for C_2H_6. At a voltage of -1.7 V (Ag/AgCl), this catalyst demonstrates a significantly greater efficiency for producing C_2H_6 compared to Cu NAs, with a five-fold increase. Empirical data indicates that the Cu electrode doped with iodide has a higher affinity for C_2H_4 adsorption and superior capacity to convert C_2H_4 into C_2H_6.[92] Fu-Sheng Ke and co-workers, looked into how CO_2 reduction works on electrodes made of porous Cu nanoribbon arrays (NRA) produced from CuO, or Cu NRAs. The selection for making C_2 products was greatly improved, and very little C_1 was made (less than 3%) across a wide range of potentials. Coupling between C-C atoms was facilitated at potentials below -0.701 V vs. RHE (all potentials are related to RHE), resulting in the formation of ethylene (C_2H_4), ethane (C_2H_6), and ethanol (C_2H_5OH). The overall Faradaic efficiency for C_2 exceeded 40%. The results of this study showed that CO_2 was triggered only at the surface of the copper. The presence of a copper oxide layer is most likely attributed to the reaction between copper and water that occurred during the post-analysis phase.[93] Abhijit Dutta and co-workers, designed oxide-derived (OD) copper foam catalysts for electrochemical CO_2 conversion via HER-assisted electrodeposition. The most optimal C_2 efficiencies are recorded at a voltage of -0.8 V, with a resulting FEC_2 value of 55%. The CO_2 electrolysis investigations conducted on various Cu foam catalysts provide additional evidence of the significant influence of the surface pore size diameter (thickness of the catalyst) on the FEC_2 values. In addition to the existence of active surface sites that promote the combination of *CO molecules, we observe that the temporary confinement of gaseous intermediates (CO, H_2, C_2H_4) within the mesoporous foam is a crucial component in explaining the preference for the completely reduced C_2 product (C_2H_6).[94] Sujat Sen and co-workers, designed the copper foams with a three-dimensional structure by using electrodeposition on copper surfaces that had been physically polished, resulting in an electrode with

hierarchical porosity. These nanofoams have been found to have a significant impact on the mechanism of CO_2 electroreduction, as supported by experimental findings. These include an enhanced faradaic efficiency for formate at all potentials, as well as a reduced faradaic efficiency for CO, CH_4, and C_2H_4. Additionally, the nanofoams promote the production of saturated hydrocarbons, specifically C_2H_6, and generate novel C_3 products, namely C_3H_6.[95] Chung Shou Chen and co-workers, to reduce CO_2 to C_2H_6, through C_2H_4 intermediates, design an electrochemical system with Cu_2O-derived Cu working electrodes and $PdCl_2$ dopants. The selection of $PdCl_2$ was based on its established capability to serve as a support for active hydrogen and its efficient binding to olefins. An applied potential of -1.0 V resulted in a substantial ethane generation with a faradic efficiency of up to 30.1%. Elaborate mechanistic investigations unequivocally establish that C_2H_4 was initially generated by the reduction of CO_2 at the Cu sites. Subsequently, it was subjected to hydrogenation with the aid of adsorbed $PdCl_x$, resulting in the formation of C_2H_6. Both copper and $PdCl_x$ sites are necessary for the effective conversion of C_2H_4 to C_2H_6. Introducing other types of palladium-based particles, such as Pd^0, PdO, or $Pd–Al_2O_3$, to the electrolyte did not result in the same level of conversion efficiency. Introducing $PdCl_2$ dopants in conjunction with a copper working electrode is a novel approach to broaden the range of compounds that can be synthesised using CO_2 as building blocks. Therefore, we anticipate that the concepts outlined in this document will create opportunities for the conversion of carbon dioxide into more intricate compounds.[96] Dohyung Kim and co-workers demonstrated that a collection of closely packed copper nanoparticles (NPs) can facilitate the targeted transformation of CO_2 into compounds with multiple carbon atoms, while effectively reducing the production of compounds with a single carbon atom. The Cu NP ensemble undergoes a structural transition during electrolysis, resulting in the creation of cube-like structures that are catalytically active and capable of producing ethylene, ethanol, and n-propanol. These structures have the ability to produce C_2 and C_3 products simultaneously with modest overpotentials in neutral pH aqueous solutions, demonstrating the significance of in situ structural changes in CO_2 electrocatalysis.[97] Dunfeng Gao and co-workers electrochemically synthesised in KCl and low-pressure plasma processes were used to make Cu nanocube catalysts that could be changed in their shape, the amount of defects they contained, and the amount of oxygen they housed. These catalysts demonstrate significantly increased activity and selectivity towards ethylene and alcohol (with the maximum Faradaic efficiency of around 45% for ethylene, approximately 22% for ethanol, and a total of approximately 73% for all C_2 and C_3 products), along with lower onset potentials in comparison to the electropolished Cu foil. Their catalytic characteristics may be adjusted by modifying their shape and defect density, ion content, and surface roughness by plasma-induced changes. Through the examination of the relationship between the catalytic efficiency and the surface characteristics and composition of catalysts treated in various ways, we have shown that the existence of imperfections, as well as oxygen species on the surface and beneath it, including oxygen ions connected to Cu^+ species, is

a crucial factor in achieving both high activity and ethylene selectivity. This factor is even more significant than the presence of Cu(100) facets.[98] Mohamed Ebaid and co-workers described a new way to make highly roughened mesoporous Cu catalysts that are very different from the single-crystalline Cu electrodes made by the Bridgeman method or metal-ion battery cycling, as well as the Cu_2O-oriented films that are electrochemically deposited on Cu substrates. The mesoporous Cu catalyst has exceptional performance for aqueous CO_2RR, surpassing current standards. At a potential of -1.0 V compared to the reversible hydrogen electrode (RHE), the faradaic efficiency (FE) of multicarbon products (C_{2+}) is greater than 68%. Approximately 35% of this quantity is in the form of C_{2+} oxygenates, with around 10% being n-propanol (C_3). At a current density of around 18.5 mA cm^{-2}, only 1.1% carbon monoxide (CO) is produced and there is no measurable amount of methane. Cu_3N films with consistent properties are generated using the process of thermal nitriding of Cu foil at atmospheric pressure using a stream of NH_3/O_2. During CO_2RR, the Cu_3N precursor undergoes reduction and transforms into a metallic Cu structure that has a very porous nature. This metallic Cu structure has an electrochemical surface roughness more than 17, which is significantly higher than that of an electropolished Cu foil. The exceptional carbon dioxide reduction reaction (CO_2RR) efficiency of Cu generated from Cu_3N can be attributed to a significant abundance of Cu sites with low coordination, as well as an elevation in surface pH resulting from the local reaction environment.[99]Minfang Wu and co-workers, synthesised a three-dimensional nanodendritic Cu structure from commercially available Cu particles using a wet-chemistry reaction and in situ electrochemical reconfiguration. Copper particles were scattered across the large-scale two-dimensional nanosheets in copper phosphate. These particles then developed into highly branching copper nanodendrites during the early stage of CO_2RR. The Cu nanodendrites (Cu NDs) that were prepared demonstrated exceptional and consistent performance in converting CO_2 to ethylene and C_3 (n-PrOH and propanal). This was due to the formation of a plentiful conductive network and a large active surface area. The Cu NDs achieved ethylene yields that were 70-120% higher and C_3 yields that were 60-220% higher compared to spherical Cu particles. Additionally, the Cu NDs exhibited a reduction of more than 20% in H_2 FE. Furthermore, the initial potentials for the synthesis of C_3 products were reduced by 200 mV, and the production of methane was inhibited on the Copper Nanodots (Cu NDs).[100]

Table 3 Electrochemical CO_2 Reduction Performances of Cu-Based Catalyst.

S. No	Catalyst	FE (%)	Potential (vs RHE)	Electrolyte	Current Density	Stability hours	Main Product	ref
1	Single Cu atom	36.7%	-0.76 V	0.1 M $KHCO_3$	1.0 mA cm^{-2}	5	Acetone	[62]

2	$dCu_2O/Ag_{2.3\%}$	40.8%	-0.87 V	1 M KOH	326.4 mA cm^{-2}	12	Ethanol	[63]
3	Cu-NC	18.4 %	-1.01 V	0.1 M $KHCO_3$	-	8	Ethanol	[65]
4	Cu_2O/NCS	24.7%	-1.3 V	0.1 M $KHCO_3$	-	4	Ethylene	[101]
5	CuN_4	55%	-1.2 V	0.1 M $CsHCO_3$	16.2 mA/cm^2	1	Ethanol	[66]
6	Cu_1Ni_2@N-MWCNT	90%	-0.53 V	0.5 M $KHCO_3$	3.0 mF cm^{-2}	10	Formate	[46]
7	Cu-doped carbon xerogel	-	-	0.1 M $KHCO_3$	-	5	Methane	[47]
8	Cu-nanoparticles	54 %	-1.0 V	0.1 M $KHCO_3$	6.53 mF cm^{-2}	12	Formate	[52]
9	GO-VB_6-Cu-2	56.3%	-0.250 V	0.1 M $KHCO_3$	7.452 mA/cm^2	24	Ethanol	[68]
10	Cu-N-C	92%	-0.7 V	0.1 M $KHCO_3$	3.61 mA cm^{-2}	60	Carbon monoxide	[53]
11	Cu_2O@ Cu-MOF	79.4%	-1.71 V	0.1 M $KHCO_3$	8.4 mA cm^{-2}	1	Methane	[70]
12	PcCu-Cu-O	50%	-1.2 V	0.1 M $KHCO_3$	7.3 mA cm^{-2}	4	Ethylene	[55]
13	$Cu_{90}In_{10}$/C	85%	-0.75 V	0.1 M $KHCO_3$	9.85 mF cm^{-2}	4	Carbon monoxide	[54]
14	CuO/CuTCPP	85.2%	-1.65 V	0.5 M $EMIMBF_4$	4.5 mA cm^{-2}	5	Formic acid	[57]
15	Cu(111)@Cu-THQ	42%	-1.4 V	0.1 M $KHCO_3$	14.3 mA cm^{-2}	8	Ethylene	[69]
16	CuZn	25%	-1.0 V	0.1 M $KHCO_3$	1.5 mA cm^{-2}	7	C_{2+}	[72]
17	Cu@CuxO	70%	-1.78 V	0.1 M $KHCO_3$	150 mA cm^{-2}	20	C_{2+}	[71]
18	Cu-Sn	90%	-0.7 V	0.1 M $KHCO_3$	4.5 mA cm^{-2}	12	Carbon monoxide	[58]
19	Cu_3N-derived Cu nanowires	86%	-1.0 V	0.1 M $KHCO_3$	–50.6 mA cm^{-2}	28	C_2	[51]
20	CuO-derived Cu	9.6 %	- 0.48 V	KH_2PO_4	−210 mA cm^{-2}	1	C_{2+}	[75]
21	Cu_v-Cu_2O	51%	-0.76 V	0.1 M $KHCO_3$	15.7 mA cm^{-2}	10	Ethylene	[79]
22	Cu-S	80%	-0.8 V	0.1 M $KHCO_3$	2.5 mA cm^{-2}	12	Formate	[48]
23	Cu-Zn	74%	-1.1 V	0.1 M $KHCO_3$	4.3 mA cm^{-2}	4	Carbon monoxide	[61]
24	Cu@$Cu_2(OH)_3$ NO	31.80%	-1.2 V	0.1 M $KHCO_3$	80 mA cm^{-2}	20	Ethylene	[73]
25	Cu_2O-derived Cu/$PdCl_2$	30.1%	-1.0 V	0.1 M $KHCO_3$	-	8	Ethylene	[74]
26	Cu_2O films	39%	-0.99 V	0.1 M $KHCO_3$	−52 mA cm^{-2}	1	C_2	[81]

27	Cu_2O-derived Cu particles	43%	-0.98 V	0.1 M $KHCO_3$	−13.3 mA cm^{-2}	1	Ethylene	[82]
28	Branched CuO nanoparticles	53%	-1.0 V	0.1 M $KHCO_3$	−22.0 mA/cm^2	12	Ethylene	[76]
29	Cu-Pd Alloy	87%	-0.9 V	0.1 M $KHCO_3$	-	5	Carbon monoxide	[56]
30	Cu-Pt Alloy	21%	-1.6 V	0.5 M $KHCO_3$	0.598 mA cm^{-2}	0.5	Methane	[59]
31	CuMgAl LDH	-	-0.4 V	0.3 M $KHCO_3$	-	24	Acetic acid	[83]
32	PD-CuO_x/C	45%	−1.4 V	0.1 M $KHCO_3$	26.0 mA cm^{-2}	48	Ethylene	[84]
33	$CuCo_2Se_4$	100%	-0.25 V	0.3 M $NaHCO_3$	26 mA cm^{-2}	100	Acetate	[85]
34	Cu(salophen)-coated GDE	37%	−1.2V	1 M KOH	121 mA cm^{-2}	2	C_{2+}	[86]
35	Ag–Cu_2O	70%	-0.9 V	1 M KOH	310 mA cm^{-2}	20	Acetic acid	[90]
36	hydroxo-bridged phenanthroline Cu (II) molecule	42%	−1.25 V	0.1 M $CsHCO_3$	−5.5 mA cm^{-2}	15	Ethylene	[87]
37	Cu NC spheres	41%	−1.1 V	0.1 M $KHCO_3$	−9 mA cm^{-2}	1	Ethylene	[88]
38	Copper electrodes	45%	−1.2 V	0.1 M $KHCO_3$	5 mA cm^{-2}	8	Methane	[91]
39	Oxygen-bearing copper	45%	−0.95 V	0.3 M $NaHCO_3$	44.7 mA cm^{-2}	1	Ethylene	[89]
40	Nano defective Cu nanosheets	83.2%	−1.0 V	0.1 M K_2SO_4	66.5 mA cm^{-2}	1	Ethylene	[102]

Summary and Perspectives:

Though researchers have identified electrocatalytic CO_2 reduction technology as one of the most promising technologies for reducing CO_2 emissions and achieving carbon neutrality, perfecting a single electrolysis system component does not necessarily result in an improvement in the overall performance. Additionally, the electrolysis system presenting auxiliary facilities are insufficient to meet industrial demands. There is a significant barrier in cost reduction, obtaining bulk chemicals from the CO_2 reduction on the market, upstream CO_2 supply, and downstream product purification. On the other hand, the present energy system must undergo significant changes to accommodate the goal of CO_2 emission reductions and carbon neutrality. Here, we outline current scenario for the full industrial chain of the CO_2 reduction based on state-of-the-art technology. The global energy industry might be reorganised to close the anthropogenic carbon cycle by achieving high performance in the CO_2RR, comprehending its mechanics, and connecting it to

renewable energy sources, like wind or solar. We presented an overview of the CO_2RR electrocatalysis using Cu-based catalysts with an emphasis on their design, synthesis, characterization, and mechanisms. Although the electrochemical CO_2RR is a very alluring prospect for future study and potential commercial use, there are still certain issues that must be resolved before wide-scale deployment. Research on catalysts that can dependably yield higher value products is essential since syngas products require more workup. The production of these higher value compounds has received a lot of attention, but research on C_2 and higher carbon products is scarce. This calls for the discovery of additional and advanced catalysts that can consistently convert CO_2 into C_2 products or higher. This will make it possible to get rid of unnecessary processes like the Fischer-Tropsch that could have a detrimental influence on the environment. Importantly, more study into 2D carbide and nitride catalysts is required in order to better understand them and advance them in this growing technology due to the limited works and potential for becoming excellent CO_2RR electrocatalysts. They have proven to be extremely effective support systems for other catalysts, but nothing is known about how well they act on their own in the CO_2RR, which limits their potential application. Additionally, theoretical studies have demonstrated the tremendous potential of these novel catalysts for the CO_2RR in the future. While DFT calculations are capable of discovering prospective catalysts, they are limited to reporting theoretical values. As a result, experimental work must be conducted in addition to DFT calculations to thoroughly assess potential catalysts. To validate or correct the DFT calculations and better understand the catalyst, which will enable better designing of catalysts in the future, *in situ* characterisation and testing must be carried out in addition to the experimental work. Machine learning might be used to expeditiously complete additional high-throughput screening procedures in addition to carrying out experimental work to verify DFT calculations. Any flaws in DFT calculations and experimental work might be corrected with the proper application of machine learning.

To summarise, to combat climate change and maintain a sustainable future for future generations, the pursuit of CO_2 reduction measures is of utmost importance. Through this analysis, we have examined several methods and innovations for reducing carbon dioxide emissions, including carbon capture, sustainable land use, and transportation improvements. There is no one answer those fits all for the difficult problem of reducing CO_2; rather, a comprehensive strategy that incorporates these several approaches is required. It is obvious that the chances for reducing CO_2 are both positive and difficult as we look to the future. The incredible developments in renewable energy technology, the rising popularity of electric cars, and the expanding understanding of the need of sustainable business practises across industries all point to a positive future. But the obstacles are just as great, particularly when it comes to tackling the global dimension of climate change, managing the political environment, and ensuring that everyone has access to sustainable solutions.

Acknowledgements

The authors appreciate the support from SRM Institute of Science and Technology, India.

Conflict of Interest

The authors declare no conflict of interest.

Author Contributions

Manova Santhosh Yesupatham: Investigation, writing - draft, review. Brahmari Honnappa: Investigation, writing - draft, review. Nithish Agamendran: writing – draft. S. Sai Yeswanth kumar: writing – draft. Gayathri Chellasamy: review, and editing. Saravanan Govindaraju: review, and editing. Kyusik Yun: review, and editing. Clament Sagaya Selvam: review, writing, and editing. Arthanareeswari. M: review and editing. We Li: review. Karthikeyan Sekar: Investigation, review, resources, and editing.

Acknowledgements

K.S. would like to thank the Royal Society-Newton International Fellowship Alumni follow-on funding support AL\211016 and AL\221024. K.S. would like to thank Department of Chemistry at SRM- Institute of Science and Technology. K.S. also thanks to the SERB Start-up Research Grant (SRG/2023/000658).

References:

[1] aD. L. McCollum, W. Zhou, C. Bertram, H.-S. De Boer, V. Bosetti, S. Busch, J. Després, L. Drouet, J. Emmerling, M. J. N. E. Fay, **2018**, *3*(7), 589-599; bP. IEA, in *Technical Report*, **2020**; cG. P. Peters, R. M. Andrew, J. G. Canadell, S. Fuss, R. B. Jackson, J. I. Korsbakken, C. Le Quéré, N. J. N. C. C. Nakicenovic, **2017**, *7*(2), 118-122.
[2] B. Zhang, Y. Zhang, X. Zhao, J. J. E. s. F. Meng, **2018**, *6*(1), 103-116.
[3] aJ. Rogelj, M. Den Elzen, N. Höhne, T. Fransen, H. Fekete, H. Winkler, R. Schaeffer, F. Sha, K. Riahi, M. J. N. Meinshausen, **2016**, *534*(7609), 631-639; bH. Kanaboshi, F. Sano, J. Oda, K. Akimoto, N. J. E. Onishi, C. Change, **2021**, *2*, 100027; cJ. Rogelj, D. Huppmann, V. Krey, K. Riahi, L. Clarke, M. Gidden, Z. Nicholls, M. J. N. Meinshausen, **2019**, *573*(7774), 357-363.
[4] aF. Bazzaz, J. Coleman, S. J. C. J. o. F. R. Morse, **1990**, *20*(9), 1479-1484; bN. C. Baso, J. A. Coetzee, B. S. Ripley, M. P. J. A. B. Hill, **2021**, *170*, 103348; cS. Choi, J. H. Drese, P. M. Eisenberger, C. W. J. E. s. Jones, technology, **2011**, *45*(6), 2420-2427.
[5] aH. H. Khoo, R. B. J. E. Tan, fuels, **2006**, *20*(5), 1914-1924; bN. J. I. J. o. H. E. Muradov, **1993**, *18*(3), 211-215; cB. A. Gyamfi, I. Ozturk, M. A. Bein, F. V. J. B. Bekun, Bioproducts, Biorefining, **2021**, *15*(3), 840-851; dJ. Rajendran, B. H. Shetty, D. Ganapathy, P. Murugan, R. Atchudan, D. Umapathy, A. Khosla, A. K. Sundramoorthy, *Journal of The Electrochemical Society* **2022**, *169*(1), 017515.
[6] aT.-L. Kim, H. Lim, H. Chung, K. Veerappan, C. J. P. Oh, **2022**, *11*(24), 3530; bT. Wieloch, A. Augusti, J. J. N. P. Schleucher, **2023**; cJ. Y. Leung, S. Zhang, S. D. J. S. Connell, **2022**, *18*(35), 2107407.
[7] aB. Verma, S. Kumar, R. Sharma, S. J. Borah, A. Gupta, M. K. Gupta, R. Kumar, K. K. Dubey, Y. K. Mishra, V. J. S. E. Kumar, Fuels, **2023**; bM. M. Kandy, M. Sankaralingam, **2022**; cG. Lekshmi, K. Bazaka, S. Ramakrishna, V. J. M. H. Kumaravel, **2023**, *10*(2), 292-312.
[8] aL. Li, X. Li, Y. Sun, Y. J. C. S. R. Xie, **2022**, *51*(4), 1234-1252; bY. Ma, X. Yi, S. Wang, T. Li, B. Tan, C. Chen, T. Majima, E. R. Waclawik, H. Zhu, J. J. N. C. Wang, **2022**, *13*(1), 1400; cT. A. J. R. a. Saleh, **2022**, *12*(37), 23869-23888.

[9] aX. An, Q. Tang, H. Lan, H. Liu, X. Yu, J. Qu, H. Lin, J. J. A. C. Ye, **2022**, *134*(46), e202212706; bY. Nie, T. Bo, W. Zhou, H. Hu, X. Huang, H. Wang, X. Tan, L. Liu, J. Ye, T. J. J. o. M. C. A. Yu, **2023**, *11*(4), 1793-1800; cW. Zhou, S. R. Docherty, C. Ehinger, X. Zhou, C. J. C. S. Copéret, **2023**, *14*(20), 5379-5385.
[10] aM. He, Y. Sun, B. J. A. C. Han, **2022**, *134*(15), e202112835; bI. J. T. C. R. Khan, **2022**, *22*(1), e202100219; cA. Kumar, V. Hasija, A. Sudhaik, P. Raizada, Q. Van Le, P. Singh, T.-H. Pham, T. Kim, S. Ghotekar, V.-H. J. C. E. J. Nguyen, **2022**, *430*, 133031.
[11] aZ. Yu, Y. Li, A. Torres-Pinto, A. P. LaGrow, V. M. Diaconescu, L. Simonelli, M. J. Sampaio, O. Bondarchuk, I. Amorim, A. J. A. C. B. E. Araujo, **2022**, *310*, 121318; bM. Ramadoss, M. A. Pandit, Y. Chen, M. Karpuraranjith, M. Krishnamurthi, in *Noble Metal-Free Electrocatalysts: Fundamentals and Recent Advances in Electrocatalysts for Energy Applications. Volume 1*, ACS Publications, **2022**, pp. 227-255; cM. S. Yesupatham, A. Augustin, N. Agamendran, B. H. Honnappa, M. Shanmugam, P. J. Sagayaraj, T. Ganesan, N. C. S. Selvam, K. J. S. E. Sekar, Fuels, **2023**.
[12] K. C. Poon, W. Y. Wan, H. Su, H. J. R. a. Sato, **2022**, *12*(35), 22703-22721.
[13] Z. Chen, Z. Liu, X. J. N. C. Xu, **2023**, *14*(1), 936.
[14] aG. H. Han, J. Bang, G. Park, S. Choe, Y. J. Jang, H. W. Jang, S. Y. Kim, S. H. J. S. Ahn, **2023**, *19*(16), 2205765; bD. Bagchi, S. Roy, S. C. Sarma, S. J. A. F. M. C. Peter, **2022**, *32*(51), 2209023; cD. Giusi, M. Miceli, C. Genovese, G. Centi, S. Perathoner, C. J. A. C. B. E. Ampelli, **2022**, *318*, 121845; dM. Luo, J. Yang, X. Li, M. Eguchi, Y. Yamauchi, Z.-L. J. C. S. Wang, **2023**, *14*(13), 3400-3414.
[15] aS. Lu, Y. Zhang, M. F. Mady, W. Mekonnen Tucho, F. Lou, Z. J. I. Yu, E. C. Research, **2022**, *61*(29), 10400-10408; bB. Honnappa, S. Mohan, M. Shanmugam, A. Augustin, P. J. J. Sagayaraj, C. Chuaicham, S. Rajendran, T. K. A. Hoang, K. Sasaki, K. Sekar, *Energy Advances* **2022**, *1*(11), 738-760.
[16] K. E. Dalle, J. Warnan, J. J. Leung, B. Reuillard, I. S. Karmel, E. J. C. r. Reisner, **2019**, *119*(4), 2752-2875.
[17] D. D. Zhu, J. L. Liu, S. Z. J. A. m. Qiao, **2016**, *28*(18), 3423-3452.
[18] Z.-Y. Zhang, H. Tian, L. Bian, S.-Z. Liu, Y. Liu, Z.-L. J. J. o. E. C. Wang, **2023**, *83*, 90-97.
[19] aG. Zhao, X. Huang, X. Wang, X. J. J. o. M. C. A. Wang, **2017**, *5*(41), 21625-21649; bJ.-H. Zhou, Y.-W. J. R. C. Zhang, Engineering, **2018**, *3*(5), 591-625.
[20] J. Liu, D. Zhu, C. Guo, A. Vasileff, S. Z. J. A. E. M. Qiao, **2017**, *7*(23), 1700518.
[21] aZ. Zhang, L. Bian, H. Tian, Y. Liu, Y. Bando, Y. Yamauchi, Z. L. J. S. Wang, **2022**, *18*(18), 2107450; bB. H. Honnappa, C. Chuaicham, S. Shenoy, P. J. Sagayaraj, M. S. Yesupatham, A. Sengeni, B. Neppolian, K. Sasaki, K. J. J. o. M. C. A. Sekar, **2023**.
[22] aQ. Kong, X. An, Q. Liu, L. Xie, J. Zhang, Q. Li, W.-T. Yao, A. Yu, Y. Jiao, C. J. M. H. Sun, **2023**; bB. Jiang, Y. Guo, F. Sun, S. Wang, Y. Kang, X. Xu, J. Zhao, J. You, M. Eguchi, Y. J. A. n. Yamauchi, **2023**, *17*(14), 13017-13043.
[23] X. Peng, L. Zeng, D. Wang, Z. Liu, Y. Li, Z. Li, B. Yang, L. Lei, L. Dai, Y. J. C. S. R. Hou, **2023**.
[24] B. G. Ghule, J.-H. J. E. Jang, Fuels, **2023**.
[25] X. Zhao, L. Du, B. You, Y. J. C. S. Sun, Technology, **2020**, *10*(9), 2711-2720.
[26] A. D. Handoko, F. Wei, Jenndy, B. S. Yeo, Z. W. J. N. C. Seh, **2018**, *1*(12), 922-934.
[27] aT. N. Nguyen, C.-T. J. C. S. R. Dinh, **2020**, *49*(21), 7488-7504; bT. Tang, Z. Wang, J. J. A. F. M. Guan, **2022**, *32*(19), 2111504.
[28] S. Popović, M. Smiljanić, P. Jovanovič, J. Vavra, R. Buonsanti, N. J. A. C. Hodnik, **2020**, *132*(35), 14844-14854.
[29] aP. Senthilkumar, M. Mohapatra, S. J. R. a. Basu, **2022**, *12*(3), 1287-1309; bY. Yan, J. Miao, Z. Yang, F.-X. Xiao, H. B. Yang, B. Liu, Y. J. C. S. R. Yang, **2015**, *44*(10), 3295-3346.
[30] S. Nitopi, E. Bertheussen, S. B. Scott, X. Liu, A. K. Engstfeld, S. Horch, B. Seger, I. E. Stephens, K. Chan, C. J. C. r. Hahn, **2019**, *119*(12), 7610-7672.
[31] A. Kaur, R. Sharma, R. J. J. o. G. E. Bharti, **2020**, *10*, 7399-7421.
[32] M. J. Bogard, P. A. J. G. B. C. del Giorgio, **2016**, *30*(10), 1509-1525.
[33] N. J. N. RE, **2022**, *603*.
[34] C. N. Waters, J. Zalasiewicz, C. Summerhayes, I. J. Fairchild, N. L. Rose, N. J. Loader, W. Shotyk, A. Cearreta, M. J. Head, J. P. J. E.-S. R. Syvitski, **2018**, *178*, 379-429.
[35] S. Shackley, C. McLachlan, C. J. C. p. Gough, **2004**, *4*(4), 377-398.
[36] S. Pattanaik, B. J. J. o. t. G. S. o. I. Nayak, **2023**, *99*(8), 1083-1093.

[37] E. U. von Weizsäcker, A. Wijkman, E. U. von Weizsäcker, A. J. C. O. C. Wijkman, Short-termism, Population, t. D. o. t. Planet, **2018**, 101-204.
[38] P. Luckow, E. A. Stanton, S. Fields, B. Biewald, S. Jackson, J. Fisher, R. J. C. Wilson, Massachusetts, **2015**.
[39] D. Yao, **2022**.
[40] aZ. Gu, H. Shen, L. Shang, X. Lv, L. Qian, G. J. S. M. Zheng, **2018**, *2*(11), 1800121; bY. Jiao, Y. Zheng, P. Chen, M. Jaroniec, S.-Z. J. J. o. t. A. C. S. Qiao, **2017**, *139*(49), 18093-18100; cE. Hayes, A. Roberson, R. J. J. o. T. E. S. Robertson, **1950**, *97*(10), 316.
[41] A. Murata, Y. J. B. o. t. C. S. o. J. Hori, **1991**, *64*(1), 123-127.
[42] P. At, M. Of, E. Reduction, *Tech. Biochem. Mol. Biol* **1990**, *20*, 5-51.
[43] X. Chen, Y. Zhao, J. Han, Y. Bu, *ChemPlusChem* **2023**, *88*(1), e202200370.
[44] aJ. E. Pander, D. Ren, Y. Huang, N. W. X. Loo, S. H. L. Hong, B. S. Yeo, *CHEMELECTROCHEM* **2018**, *5*(2), 219-237; bD. Zhong, Z. J. Zhao, Q. Zhao, D. Cheng, B. Liu, G. Zhang, W. Deng, H. Dong, L. Zhang, J. Li, J. Li, J. Gong, *Angewandte Chemie (International ed. in English)* **2021**, *60*(9), 4879-4885; cA. Vasileff, C. Xu, L. Ge, Y. Zheng, S. Z. Qiao, *Chemical communications (Cambridge, England)* **2018**, *54*(99), 13965-13968.
[45] aR. Reske, H. Mistry, F. Behafarid, B. Roldan Cuenya, P. Strasser, *Journal of the American Chemical Society* **2014**, *136*(19), 6978-6986; bA. Loiudice, P. Lobaccaro, E. A. Kamali, T. Thao, B. H. Huang, J. W. Ager, R. Buonsanti, *Angewandte Chemie (International ed. in English)* **2016**, *55*(19), 5789-5792; cC. W. Lee, K. D. Yang, D. H. Nam, J. H. Jang, N. H. Cho, S. W. Im, K. T. Nam, *Advanced Materials* **2018**, *30*(42), 1704717; dK. Mori, T. Sano, H. Kobayashi, H. Yamashita, *Journal of the American Chemical Society* **2018**, *140*(28), 8902-8909; eS. Y. Lee, H. Jung, N. K. Kim, H. S. Oh, B. K. Min, Y. J. Hwang, *Journal of the American Chemical Society* **2018**, *140*(28), 8681-8689; fA. Bhardwaj, J. Kaur, M. Wuest, F. Wuest, *Nature communications* **2017**, *8*(1), 1; gC. He, D. Duan, J. Low, Y. Bai, Y. Jiang, X. Wang, S. Chen, R. Long, L. Song, Y. Xiong, *Nano Research* **2023**, *16*(4), 4494-4498; hZ. Yin, C. Yu, Z. Zhao, X. Guo, M. Shen, N. Li, M. Muzzio, J. Li, H. Liu, H. Lin, J. Yin, G. Lu, D. Su, S. Sun, *Nano letters* **2019**, *19*(12), 8658-8663.
[46] M. Wang, Z. Cai, B. Zhang, K. Yang, T. Shou, M. T. Bernards, P. Xie, Y. He, Y. J. E. Shi, Fuels, **2022**, *36*(11), 5833-5842.
[47] A. F. Pérez-Cadenas, C. H. Ros, S. Morales-Torres, M. Pérez-Cadenas, P. J. Kooyman, C. Moreno-Castilla, F. J. C. Kapteijn, **2013**, *56*, 324-331.
[48] T. Shinagawa, G. O. Larrazábal, A. J. Martín, F. Krumeich, J. J. A. C. Perez-Ramirez, **2018**, *8*(2), 837-844.
[49] W. Ju, A. Bagger, G.-P. Hao, A. S. Varela, I. Sinev, V. Bon, B. Roldan Cuenya, S. Kaskel, J. Rossmeisl, P. J. N. c. Strasser, **2017**, *8*(1), 944.
[50] X. Zhang, Y. Zhang, F. Li, C. D. Easton, A. M. Bond, J. J. N. R. Zhang, **2018**, *11*, 3678-3690.
[51] Y. Mi, S. Shen, X. Peng, H. Bao, X. Liu, J. J. C. Luo, **2019**, *6*(9), 2393-2397.
[52] S. Dongare, N. Singh, H. J. J. o. C. U. Bhunia, **2021**, *44*, 101382.
[53] F. Yang, X. Mao, M. Ma, C. Jiang, P. Zhang, J. Wang, Q. Deng, Z. Zeng, S. J. C. Deng, **2020**, *168*, 528-535.
[54] X. Ma, J. Tian, M. Wang, X. Jin, M. Shen, L. J. C. S. Zhang, Technology, **2021**, *11*(18), 6096-6102.
[55] X.-F. Qiu, H.-L. Zhu, J.-R. Huang, P.-Q. Liao, X.-M. J. J. o. t. A. C. S. Chen, **2021**, *143*(19), 7242-7246.
[56] Y. Mun, S. Lee, A. Cho, S. Kim, J. W. Han, J. J. A. C. B. E. Lee, **2019**, *246*, 82-88.
[57] J.-X. Wu, S.-Z. Hou, X.-D. Zhang, M. Xu, H.-F. Yang, P.-S. Cao, Z.-Y. J. C. S. Gu, **2019**, *10*(7), 2199-2205.
[58] Y. Zhao, C. Wang, G. G. J. J. o. M. C. A. Wallace, **2016**, *4*(27), 10710-10718.
[59] X. Guo, Y. Zhang, C. Deng, X. Li, Y. Xue, Y.-M. Yan, K. J. C. C. Sun, **2015**, *51*(7), 1345-1348.
[60] N. Yang, F. Gao, C. E. J. A. c. Nebel, **2013**, *85*(12), 5764-5769.
[61] J. Zeng, T. Rino, K. Bejtka, M. Castellino, A. Sacco, M. A. Farkhondehfal, A. Chiodoni, F. Drago, C. F. J. C. Pirri, **2020**, *13*(16), 4128-4139.
[62] K. Zhao, X. Nie, H. Wang, S. Chen, X. Quan, H. Yu, W. Choi, G. Zhang, B. Kim, J. G. J. N. c. Chen, **2020**, *11*(1), 2455.
[63] P. Wang, H. Yang, C. Tang, Y. Wu, Y. Zheng, T. Cheng, K. Davey, X. Huang, S.-Z. J. N. c. Qiao, **2022**, *13*(1), 3754.
[64] Y.-S. Cheng, X.-P. Chu, M. Ling, N. Li, K.-L. Wu, F.-H. Wu, H. Li, G. Yuan, X.-W. Wei, *Catalysis Science & Technology* **2019**, *9*(20), 5668-5675.
[65] Y.-S. Cheng, X.-P. Chu, M. Ling, N. Li, K.-L. Wu, F.-H. Wu, H. Li, G. Yuan, X.-W. J. C. S. Wei, Technology, **2019**, *9*(20), 5668-5675.

[66] D. Karapinar, N. T. Huan, N. Ranjbar Sahraie, J. Li, D. Wakerley, N. Touati, S. Zanna, D. Taverna, L. H. Galvão Tizei, A. J. A. C. I. E. Zitolo, **2019**, *58*(42), 15098-15103.
[67] A. V. Rayer, E. Reid, A. Kataria, I. Luz, S. J. Thompson, M. Lail, J. Zhou, M. J. J. o. C. U. Soukri, **2020**, *39*, 101159.
[68] J. Yuan, M.-P. Yang, W.-Y. Zhi, H. Wang, H. Wang, J.-X. J. J. o. C. U. Lu, **2019**, *33*, 452-460.
[69] Z.-H. Zhao, K. Zheng, N.-Y. Huang, H.-L. Zhu, J.-R. Huang, P.-Q. Liao, X.-M. J. C. C. Chen, **2021**, *57*(95), 12764-12767.
[70] X. Tan, C. Yu, C. Zhao, H. Huang, X. Yao, X. Han, W. Guo, S. Cui, H. Huang, J. J. A. a. m. Qiu, interfaces, **2019**, *11*(10), 9904-9910.
[71] K. Yao, Y. Xia, J. Li, N. Wang, J. Han, C. Gao, M. Han, G. Shen, Y. Liu, A. J. J. o. M. C. A. Seifitokaldani, **2020**, *8*(22), 11117-11123.
[72] S. Juntrapirom, J. Santatiwongchai, A. Watwiangkham, S. Suthirakun, T. Butburee, K. Faungnawakij, P. Chakthranont, P. Hirunsit, B. J. C. S. Rungtaweevoranit, Technology, **2021**, *11*(24), 8065-8078.
[73] M. Wang, Q. Zhang, Q. Xie, L. Wan, Y. Zhao, X. Zhang, J. J. N. Luo, **2020**, *12*(32), 17013-17019.
[74] C. S. Chen, J. H. Wan, B. S. J. T. J. o. P. C. C. Yeo, **2015**, *119*(48), 26875-26882.
[75] L. R. L. Ting, R. García-Muelas, A. J. Martín, F. L. Veenstra, S. T. J. Chen, Y. Peng, E. Y. X. Per, S. Pablo-García, N. López, J. J. A. C. Pérez-Ramírez, **2020**, *132*(47), 21258-21265.
[76] J. Kim, W. Choi, J. W. Park, C. Kim, M. Kim, H. J. J. o. t. A. c. s. Song, **2019**, *141*(17), 6986-6994.
[77] A. N. Grace, S. Y. Choi, M. Vinoba, M. Bhagiyalakshmi, D. H. Chu, Y. Yoon, S. C. Nam, S. K. J. A. e. Jeong, **2014**, *120*, 85-94.
[78] M. Wu, C. Zhu, K. Wang, G. Li, X. Dong, Y. Song, J. Xue, W. Chen, W. Wei, Y. J. A. a. m. Sun, interfaces, **2020**, *12*(10), 11562-11569.
[79] X. Ren, X. Zhang, X. Cao, Q. J. J. o. C. u. Wang, **2020**, *38*, 125-131.
[80] Y. Huang, A. D. Handoko, P. Hirunsit, B. S. J. A. c. Yeo, **2017**, *7*(3), 1749-1756.
[81] D. Ren, Y. Deng, A. D. Handoko, C. S. Chen, S. Malkhandi, B. S. J. A. C. Yeo, **2015**, *5*(5), 2814-2821.
[82] A. D. Handoko, C. W. Ong, Y. Huang, Z. G. Lee, L. Lin, G. B. Panetti, B. S. J. T. J. o. P. C. C. Yeo, **2016**, *120*(36), 20058-20067.
[83] M. Serafini, F. Mariani, A. Fasolini, E. T. Brandi, E. Scavetta, F. Basile, D. J. A. F. M. Tonelli, **2023**, 2300345.
[84] T. Gao, Y. Gu, M. Wu, Y. Liu, L. Yang, T. Han, S. Zhang, S. Li, W. Wei, W. J. E. Chen, Fuels, **2023**.
[85] A. Saxena, S. Kapila, J. E. Medvedeva, M. J. A. A. M. Nath, Interfaces, **2023**, *15*(11), 14433-14446.
[86] L.-J. Zhu, D.-H. Si, F.-X. Ma, M.-J. Sun, T. Zhang, R. J. A. C. Cao, **2023**, *13*(8), 5114-5121.
[87] N. Liu, S. Bartling, A. Springer, C. Kubis, O. S. Bokareva, E. Salaya, J. Sun, Z. Zhang, S. Wohlrab, A. J. A. M. Abdel-Mageed, **2023**, 2309526.
[88] A. Loiudice, P. Lobaccaro, E. A. Kamali, T. Thao, B. H. Huang, J. W. Ager, R. J. A. C. I. E. Buonsanti, **2016**, *55*(19), 5789-5792.
[89] W. Zhang, C. Huang, Q. Xiao, L. Yu, L. Shuai, P. An, J. Zhang, M. Qiu, Z. Ren, Y. J. J. o. t. A. C. S. Yu, **2020**, *142*(26), 11417-11427.
[90] R. Dorakhan, I. Grigioni, B.-H. Lee, P. Ou, J. Abed, C. O'Brien, A. Sedighian Rasouli, M. Plodinec, R. K. Miao, E. J. N. S. Shirzadi, **2023**, *2*(5), 448-457.
[91] Y. Hori, A. Murata, R. J. J. o. t. C. S. Takahashi, Faraday Transactions 1: Physical Chemistry in Condensed Phases, **1989**, *85*(8), 2309-2326.
[92] K. Xiang, Y. Liu, C. Li, X. Liu, H. Yi, L. Wu, F. Shen, M. Liu, P. Wang, H. Liu, *Energy & Fuels* **2021**, *35*(19), 15987-15994.
[93] F.-S. Ke, X.-C. Liu, J. Wu, P. P. Sharma, Z.-Y. Zhou, J. Qiao, X.-D. Zhou, *Catalysis Today* **2017**, *288*, 18-23.
[94] A. Dutta, M. Rahaman, N. C. Luedi, M. Mohos, P. Broekmann, *ACS Catalysis* **2016**, *6*(6), 3804-3814.
[95] S. Sen, D. Liu, G. T. R. Palmore, *ACS Catalysis* **2014**, *4*(9), 3091-3095.
[96] C. S. Chen, J. H. Wan, B. S. Yeo, *The Journal of Physical Chemistry C* **2015**, *119*(48), 26875-26882.
[97] D. Kim, C. S. Kley, Y. Li, P. Yang, *Proceedings of the National Academy of Sciences* **2017**, *114*(40), 10560-10565.
[98] D. Gao, I. Zegkinoglou, N. J. Divins, F. Scholten, I. Sinev, P. Grosse, B. Roldan Cuenya, *ACS Nano* **2017**, *11*(5), 4825-4831.

[99] M. Ebaid, K. Jiang, Z. Zhang, W. S. Drisdell, A. T. Bell, J. K. Cooper, *Chemistry of Materials* **2020**, *32*(7), 3304-3311.
[100] M. Wu, C. Zhu, K. Wang, G. Li, X. Dong, Y. Song, J. Xue, W. Chen, W. Wei, Y. Sun, *ACS Applied Materials & Interfaces* **2020**, *12*(10), 11562-11569.
[101] H. Ning, X. Wang, W. Wang, Q. Mao, Z. Yang, Q. Zhao, Y. Song, M. J. C. Wu, **2019**, *146*, 218-223.
[102] P. De Luna, R. Quintero-Bermudez, C.-T. Dinh, M. B. Ross, O. S. Bushuyev, P. Todorović, T. Regier, S. O. Kelley, P. Yang, E. H. J. N. C. Sargent, **2018**, *1*(2), 103-110.